SOVIET MATERIAL ON INTERNAL WAVE EFFECTS

Stuart G. Hibben

Informatics, Incorporated

Prepared for:

Air Force Office of Scientific Research
Advanced Research Projects Agency

30 April 1974

AFOSR - TR - 74 - 0798	AD 779931
4. TITLE (and Subtitle) Soviet Material on Internal Wave Effects	5. TYPE OF REPORT & PERIOD COVERED Scientific . . . Interim 6. PERFORMING ORG. REPORT NUMBER
7. AUTHOR(s) Stuart G. Hibben	8. CONTRACT OR GRANT NUMBER(s) F44620-72-C-0053
9. PERFORMING ORGANIZATION NAME AND ADDRESS Informatics Inc. 6000 Executive Boulevard Rockville, Maryland 20852	10. PROGRAM ELEMENT, PROJECT, TASK AREA & WORK UNIT NUMBERS ARPA Order No. 1624 Program Code No. 62701EE10
11. CONTROLLING OFFICE NAME AND ADDRESS Defense Advance Research Projects Agency/STO 1400 Wilson Boulevard Arlington, Virginia 22209	12. REPORT DATE April 30, 1974 13. NUMBER OF PAGES 84
14. MONITORING AGENCY NAME & ADDRESS(if different from Controlling Office) A. F. Office of Scientific Research/NP 1400 Wilson Boulevard Arlington, Virginia 22209	15. SECURITY CLASS. (of this report) Unclassified 15a. DECLASSIFICATION DOWNGRADING SCHEDULE

16. DISTRIBUTION STATEMENT (of this Report)

Approved for public release; distribution unlimited.

17. DISTRIBUTION STATEMENT (of the abstract entered in Block 20, if different from Report)

18. SUPPLEMENTARY NOTES

Scientific . . . Interim

19. KEY WORDS (Continue on reverse side if necessary and identify by block number)

Internal Waves
Capillary Waves
Surface Signature
Turbulent Flow
Ocean Microstructure

20. ABSTRACT (Continue on reverse side if necessary and identify by block number)

This is a collection of abstracts of recent Soviet articles on generation and detection of internal waves. It is based mainly on items listed in the January 1, 1974 Bibliography of Soviet Material on Internal Waves which were indicated as being of potential interest. Several items from this Bibliography were judged important enough to warrant full translation, which was done elsewhere and are not included herein.

The abstracts are divided into internal effects, and surface effects comprising active and passive measurement of wave states.

DD FORM 1 JAN 73 1473 EDITION OF 1 NOV 65 IS OBSOLETE

UNCLASSIFIED
SECURITY CLASSIFICATION OF THIS PAGE (When Data Entered)

SOVIET MATERIAL ON INTERNAL WAVE EFFECTS

Sponsored by

Advanced Research Projects Agency

ARPA Order No. 1622-4

April 30, 1974

ARPA Order No. 1622-4
Program Code No: 62701E3F10
Name of Contractor:
Informatics Inc.
Effective Date of Contract:
January 1, 1974
Contract Expiration Date:
June 30, 1974
Amount of Contract: $137,685

Contract No. F44620-72-C-0053, P00003
Principal Investigator:
Stuart G. Hibben
Tel. (301) 770-3000 or
(301) 779-2850
Program Manager:
Klaus Liebhold
Tel: (301) 770-3000
Short Title of Work:
"Internal Waves"

This research was supported by the Advanced Research Projects Agency of the Department of Defense and was monitored by the Air Force Office of Scientific Research under Contract No. F44620-72-C-0053. The publication of this report does not constitute approval by any government organization or Informatics Inc. of the inferences, findings, and conclusions contained herein. It is published solely for the exchange and stimulation of ideas.

informatics inc
Systems and Services Company
6000 Executive Boulevard
Rockville, Maryland 20852
(301) 770-3000 Telex 89-521

ia

INTRODUCTION

This is a collection of abstracts of recent Soviet articles on generation and detection of internal waves. It is based mainly on items listed in the January 31, 1974 Bibliography of Soviet Material on Internal Waves which were indicated as being of potential interest. Several items from this Bibliography were judged important enough to warrant full translation, which was done elsewhere and are not included herein.

The abstracts are divided into internal effects, and surface effects comprising active and passive measurement of wave states.

TABLE OF CONTENTS

1. Internal Effects

Sabinin, K. D. On some characteristics of short-period internal waves in the ocean. FAiO, no. 1, 1973, 66-74.

Results are described of the spectral analysis of temperature-time series, measured in the thermocline in various regions of the Atlantic and Indian Oceans. The measurements were done from the research vessels S. Vavilov and P. Lebedev along 22 sounding lines with lengths varying from 5 to 24 miles. Special attention was paid to the analysis of the stationarity of temperature-time series.

An analysis of 10-day measurements in the North Atlantic trade current temperature-time series is characterized by nonstationarity (Fig. 1)

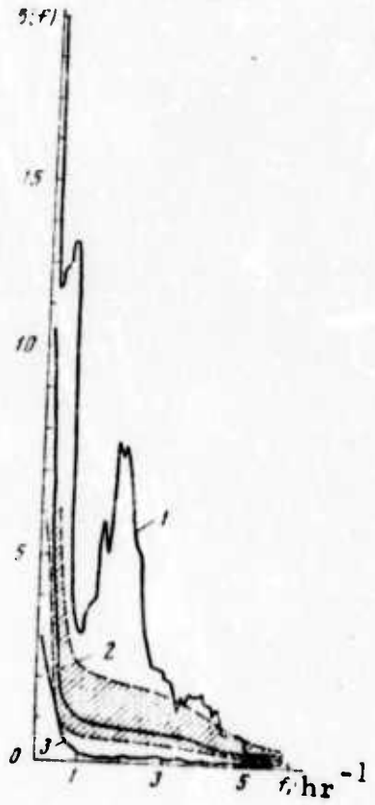

Fig. 1. Average (curve 2) and running spectra (curves 1 and 3) of temperature oscillations in the thermocline of the North Atlantic trade current. Hatched region = confidence limits.

The criterion for stationarity is expressed as a probability function P, calculations for which are shown in Fig. 2. These indicate

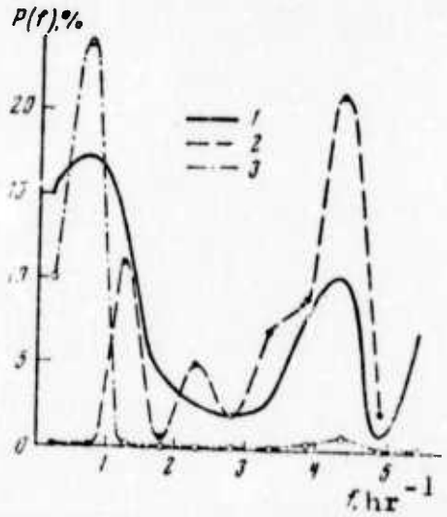

Fig. 2. Stationarity probability for temperature series measured in the Atlantic and Indian oceans.

1 - average from 16 series; 2 - northern part of the Canary current; 3 - Bay of Bengal.

a nonstationarity ($P < 1\%$) in the Bay of Bengal over almost the entire frequency range except for low frequency, and in the Canary current at low frequencies. The nonstationarity of temperature oscillations is concluded to be due to the presence of internal waves, which occur as intense wave packets subject to weak irregular fluctuations. Differences in frequency ranges are ascribed to differences in the Vaisala frequencies, namely $N = 17$ hour^{-1} in the Bay of Bengal, and $N = 4.6$ hour^{-1} in the Canary current.

The running spectra calculated for the temperature series measured in the Bay of Bengal at a depth of 100 m are shown in Fig. 3. The figure indicates that packets of 20-30 minute waves are interspersed with irregular fluctuations. An analysis of the directivity of these wave packets was made, using measurements along several sounding lines, and the average weighted values of wave parameters were determined. A

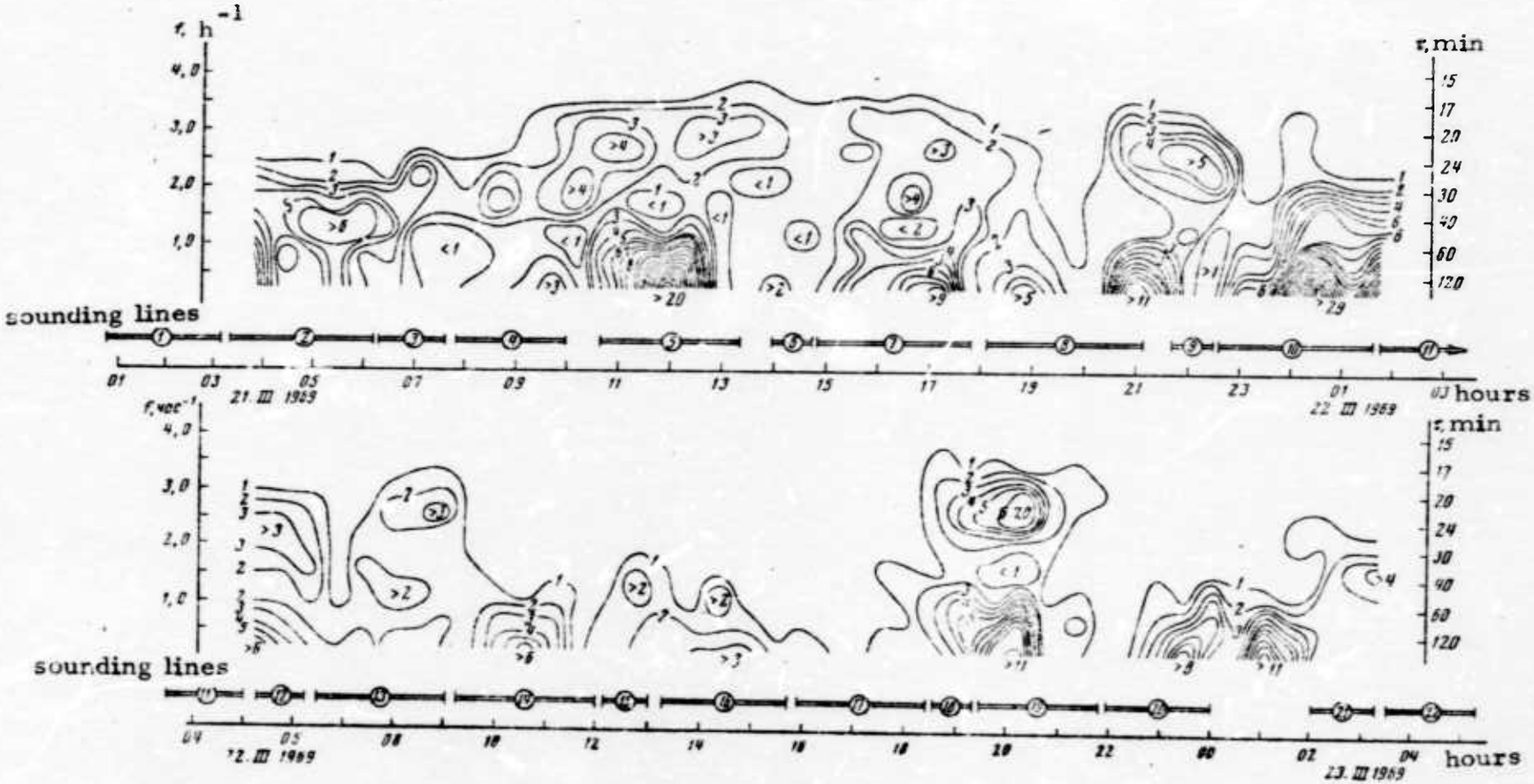

Fig. 3. Running spectrum of temperature oscillations in the thermocline of the Bay of Bengal.

comparison of experimental data and dependence of Doppler frequency on ship course calculated using these wave parameters indicates a high directivity of the 20-30 minute waves. Temperature-time series recorded by three spaced thermistor chains are illustrated in Fig. 4. The parameters of these waves were found to be: τ = 19 min, λ = 480 m, $\theta = 24^{o}$, h = 20 m and c = 40 cm/sec.

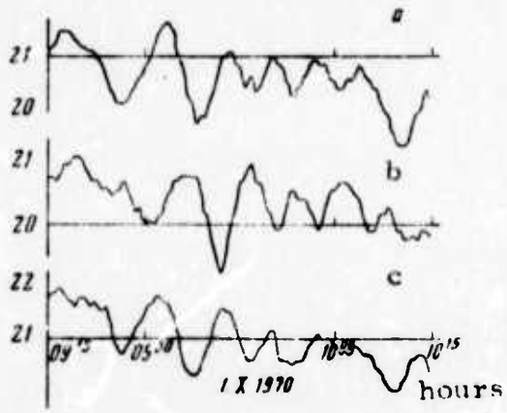

Fig. 4. Record of internal waves made from three spaced thermistor chains.

a - bow (108 m); b - buoy (106 m); c - stern (101 m).

Kononkova, G. Ye., V. A. Razumov, and I. F. Shishkin. Decay of wind waves in a medium with natural turbulence. VMU, Fiz. Astron., no. 4, 1973, 414-421.

The problem of determining the profile of a water surface versus the evolution of the pressure fluctuation field from the effect of turbulent wind is solved, with allowance for the effects of initial natural turbulence due to factors other than wind and "artificial" turbulence. The latter is assumed to cause decay of wind waves owing to wave momentum flow from the surface. The authors' experimental data confirm this assumption. Their data show that the observed decrease in wave energy occurs on account of turbulent transfer of water particles from the surface deep into the liquid mass.

The cited assumption made it possible to describe the wave development process by a closed set of equations, and to solve the set. The solution was then used to define wave spectra in the decay zone and outside of it and hence to calculate the contrast K between the wave decay zone and the background. The K value depends on degree of wave decay and the spectral ratio of the random pressure fluctuation field on the surface above the background, and in the wave decay zone. For a given water wavelength λ, the K (λ) plot will have a maximum, hence the plot of K versus the carrier frequency of an incident radar signal will also.

Kolesnikov, A. G., V. V. Yefimov, and G. N. Khristoforov. Characteristics of velocity field and wave motion in the upper ocean layer. IN: Sb. Vzaimodeystviye atmosf.i okeana. Leningrad, 1972, 61-64 (RZhGeofiz, 11/73, no. 11V51).

Various measurement data are examined in a study of linear spectral theory as applied to fundamental energetic wave components. At high frequencies, however, disagreement with this theory becomes significant. In the upper sea layer, the correlation factor of the vertical and horizontal velocity components is given as 0.2-0.3. An expression for the spectral function is derived, in good agreement with observations on the basis of separate wave and turbulent velocity fields.

Keondzhyan, V. P., and A. S. Sarkisyan. Numerical model for calculating transient flows in the sea. IN: Seminar in-ta prikl. mat. Tbilis. un-t. Annotatsii dokl, no. 7, 1973, 53-57. (RZhMekh, 10/73, no. 10B370). (Translation).

A method is described for numerical calculation of transient thermohydrodynamic characteristics of a basin with an arbitrary bottom configuration, and a shore profile located on the spherical Earth. The method is used to calculate current velocity, anomalies of sea level surface and density in the North Atlantic.

Karasev, I. F. Effect of flow turbulence on the accuracy of integrating velocities over a vertical. IN: Tr. Gos. gidrolog. in-t, no. 202, 1973, 64-73. (RZhMekh, 9/73, no. 9B899). (Translation).

Sources of error in the integrated measurement of a vertically averaged current flow are analyzed. Measurement techniques are described using a vertically moving integrating current meter or drift measurement of a rising float. With respect to accuracy of measurements, the integrating current meter appears to be clearly preferable to the integrating rising float.

Bykova, L. P. Experimental calculation of the atmospheric boundary layer characteristics for given roughness parameters of the underlying surface. IN: Trudy GGO, no. 297, 1973, 12-19. (RZhGeofiz, 12/73, no. 12B386). (Translation).

Numerical experiments for two different boundary layer models are presented and their results are compared. In the first model the properties of the underlying surface are determined by its roughness parameter only, and in the second model they are determined by the height of obstacles and the resistance coefficient which depends on distribution density of the roughness elements. A correlation obtained for the second model between dimensionless roughness and resistance parameters is found to be in satisfactory agreement with known empirical functions. In the case of sufficiently high obstacles, the roughness parameter and displacement height are correlated with wind velocity.

Gavrilov, A. S. Structure of the atmospheric boundary layer over a surface with arbitrary roughness properties. Metr. i gidrol., no. 12, 1973, 35-42.

This is a theoretical study of dynamic characteristics of the planetary atmospheric boundary layer over a horizontal surface with randomly distributed obstacles. The study n ay be used to calculate evaporation from cultivated areas and forests, or pollutant diffusion over urban areas. The mathematical analysis is based on hypotheses of a semi-empirical theory of turbulence. The obstacles are characterized by a set of averaged parameters, such as profile height and distance between the roughness elements. Characteristics of the turbulent flow are calculated within the zone of obstacles and for the boundary layer as a whole. A comparison is made between the present theoretical and earlier experimental profiles of wind and other meteorological elements.

Gurov, V. V., A. M. Gusev, and G. G. Khundzhua. Methodology and studies of small-scale turbulence near the sea-atmosphere interface. IN: Sb. Kompleks, issledovaniya prirody okeana. Moskva, Mosk. un-t, no. 4, 1973, 110-116. (RZhMekh, 11/73, no. 11B889) (Translation).

Equipment for measurement of pulsations in flow velocity, developed by the authors, is described. A mechanical sensor is used which permits measurement of all three velocity components through displacement of a sphere of special design. Recording of the displacement is made by loop oscillograph. The natural frequency of the detector is 11-15 Hz. Data are given on vertical pulsations of flow velocity at a depth of 25 cm in the Black Sea. It was shown that the pulsation distribution

is Gaussian, therefore the correlation function is represented by an exponential function. An integral time scale of turbulence α is determined from the relation $\alpha = \Delta t/n\,(n-1)$, where Δt is recording time, n = number of crossings of the pulsation trace with the average velocity. Examples are given of calculated spectral densities $G(\omega) = (2/\pi)\,\sigma^2\alpha/[1 + (\alpha\omega)^2]$, where σ^2 is the pulsation dispersion and ω is frequency.

Gatkin, N. G. Algorithms for optimal space-time processing of random fields. IN: Tr. 4-y Vses. shkoly- seminara po stat. gidro-akustike. Novosibirsk, 1973, 168-200. (RZhF, 8/73, no. 8Zh658). (Translation)

Algorithms are presented for optimal space-time processing of random signals in the presence of gaussian noise: for an accurately known signal, a signal with random initial phase, a two-component signal, or a signal with fluctuating amplitude. In addition an algorithm was considered for the processing of signals in the presence of noise produced by superposition of uncorrelated plane waves. Results are presented of a study on problems of optimal time processing of signals with different shape in the presence of non-stationary, non-white noise, as follows:

1) detection of a signal with an arbitrary amplitude and phase modulation on a background of non-stationary noise having the correlation function

$$r(t, t_1) = g_o\alpha/4\; m(t)\, m(t_1)\, e^{-\alpha(t-t_1)};$$

2) detection of a simple signal against a background of non-stationary reverberations having the correlation function

$$r(t, t_1) = \sigma_p^2\; m(t)m(t_1)\,[1 - (t-t_1)/T];$$

3) detection of a simple signal against a background of noise and stationary reverberations. Functional diagrams are presented of the systems for processing the different signals.

Faddeyev, Yu. I. Some properties of velocity potential for arbitrary motion of a variable-form body in an unbounded incompressible fluid. IN: Tr. Leningr. korablestroit. in-ta, no. 80, 1972, 93-97 (RZhMekh, 9/73, no. 9B426). (Translation).

The asymptotic expression of Sedov (Tr. Tsentr. aerogidrodinam. in-ta, no. 515, 1940) is used for the velocity potential

$$\varphi \approx -\frac{1}{4\pi}\frac{dw}{dt}\frac{1}{r} + \frac{\mathbf{er}}{r^3} \approx -\frac{1}{4\pi}\frac{dw}{dt}\frac{1}{r} + \varphi_{K7} \qquad (1)$$

where $dw/dt = Q$ is the source intensity and $r = (x^2 + y^2 + z^2)^{\frac{1}{2}}$. The dipole momentum e is determined from expressions for the momentum vector Q_f of the fluid and the velocity vector in (different) points of a body. Also, the asymptotic φ value is determined from the source distribution over the body surface. Using the condition of identity of the two asymptotic expressions, the author derives expressions for e projections and establishes a correlation between the apparent masses and intensity of sources. Determination of the source intensity reduces to solving a Fredholm integral equation of the second kind. The solution may be obtained by the method of successive approximations. In the first approximation, the expressions are used for dimensionless intensity for an equivalent triaxial ellipsoid and the method of Kostyukov is applied (Theory of ship waves and wave resistance. Sudpromgiz, 1959). The algorithm for successive approximation is presented.

Bukatov, A. Ye. Effect of ice cover on internal waves. MGI, no. 1, 1972, 53-64.

In a theoretical analysis of the title subject, a thin elastic plate is used to model an ice cover floating on the surface of a stratified fluid consisting of two layers of finite depths but different densities ρ_1 and ρ_2. The forms $\zeta 1$ and $\zeta 2$ of the waves arising at the water ice and interlayer interfaces from the effect of periodic atmospheric disturbances are expressed in terms of the ice and water layer parameters. The following three types of atmospheric disturbances are considered:

$$p_0 = af(x,y)\cos\sigma t. \quad (1),$$

$$p_0 = af(x)\cos(ky - \sigma t). \quad (2),$$

and

$$p_0 = a\cos(rx - \sigma t). \quad (3),$$

where $a = \rho_1/\rho_2$, σ and k are the velocity and wave number of the pressure wave, $r = (m^2 + n^2)^{1/2}$ in (1) and (3) and $r = (m^2 + k^2)^{1/2}$ in (2). The functions f (m, n) and f (m) are the Fourier transforms of f (x, y) and f (x), respectively.

Analysis of $\zeta 1$ and $\zeta 2$ expressions shows that ordinary surface waves and internal waves can arise at both interfaces in the cases of type (1) and (2) disturbances, but only one system of resonance waves arises at each interface for the case of a type (3) disturbance. Calculations also show that in the cases of (1) and (2), short or long period disturbances in the velocity V_2, the length λ_2, and the ratio of amplitudes of internal waves at the ice-water and interlayer interfaces, are all independent of the ice-cover parameters. The tabulated numerical V, λ, and wave amplitude data for case (1) illustrate the effects of the ice parameters and fluid inhomogeneity $\epsilon = 1-a$.

Belonosov, S. M., and I. Kh. El-Sirafi. Solution of homogeneous Navier-Stokes equations in a half-plane with a given velocity at the boundary. IN: Sb. Analit. metodi v teorii fil'tratsii i teploprovodnosti. Kiyev, 1973, 70-84. (RZhMekh, 11/73, no. 11B586). (Translation)

Nonstationary two-dimensional motion of a viscous incompressible liquid is analyzed in the half-plane y-0. Initially the liquid is stationary, its velocity at $t > 0$ in x direction is given, and velocity at infinity is zero. The complex coordinate $z = x + iy$ and the complex velocity $w = u + iv$ are used. The problem is solved by application of a Laplace transform of time and a Fourier transform of the coordinate x. The solution can be expressed by quadrature formulas.

Fedosenko, V. S. Effect of Coriolis force on nonstationary waves generated by a moving excitation source. IN: Sb. MGI, no. 1, 1973, 66-74. (RZhMekh, 12/73, no. 12B407). (Translation).

The effect of Coriolis force on a nonstationary surface and on internal waves from moving disturbances is studied in the framework of general linear wave theory. The effect on the surface waves is shown to be insignificant, whereas the internal wave elements depend significantly on the Coriolis force.

K voprosu o neutstanovivshemsya kharaktere vetrovogo volneniya v okeane (On the transient character of wind waves in the ocean). IN: Sb. Mor gidrofir. issled., no. 2(61), Sevastopol', 1973, 77-91. (RZhMekh, 12/73, no. 12B421). (Translation).

The two-dimensional problem of nonstationary motion of wind waves in the ocean is analyzed, taking into account the mechanism of energy transfer from the wind to the waves. The method of different scales was used. A dispersion relation with correction for viscosity, as well as expressions for functions of current and wave surface rise, were derived. Features of the solutions thus obtained are discussed.

Nikolayev, S. Internal waves in the seas and oceans. Morskoy sbornik, no. 10, 1973, 99-102.

A review of internal wave phenomena is given in which up-to-date results of observations and theoretical studies of internal waves are summarized and their probable causes and effects are outlined. Observations made by Soviet scientists in 1969 at the ice edge in the Chukotski Sea, and in 1970 in the North Atlantic current, have confirmed the significance of internal waves effects on various physical processes in the ocean depths, and in the regions of seasonal thermal fronts. Earthquakes and strong storms are cited as some natural phenomena which in addition to others, may trigger internal waves and might have been the cause of some submarines sinkings, specifically the French "Minerve" and the Israeli "Dikar" in 1968 and the U.S. "Thresher" in 1963. The author speculates that the latter might have hit a less dense water layer as the results of internal waves with 90 m amplitude, which were triggered at the submergence

depth by a severe storm. The Thresher may then have sustained damage which prevented it from returning to a safe depth.

It is concluded that there is a very limited possibility of forecasting high amplitude internal waves triggered by nonperiodical forces. The causes of their occurrence are not yet definitely established.

Obukhov, A. M. On the problem of nonlinear interactions in fluid dynamics. Gerlands Beitr. Geophysik, Leipzig, v. 82, 1973, no. 4, 282-290.

A turbulence mechanism is studied theoretically by analyzing dynamic models which simulate the main features of the nonlinear mechanism of energy transfer in a developed turbulent flow. The simplest analyzed model is the triplet (three interacting modes) which is based on the Burgers model and has the general properties of a fluid mechanical system, i.e., nonlinearity, conservation of energy and phase volume.

The motion of a triplet of one unstable and two stable modes is described by the Eulerian equations for a gyroscope, where the interaction parameters p, q, and r have the dimensions of wave numbers. The triplet model is applied to the study of a forced motion regime in a nonlinear system by introducing a driving force f acting on the unstable mode, and a dissipative parameter λ. The characteristics of motion will then depend on the dimensionless parameter $K = p|f|\lambda^2$, analogous to the Reynolds number. For the case of $K > 1$ (a strong f), an unstable state V becomes excited. If the sign of f changes, V also changes its sign, the mode V- is excited, while V+ vanishes, and motion is overturned. Overturning of motion is illustrated by an experiment in which mercury was driven in a three-axial

ellipsoidal cave by a rotating magnetic field. A general view of the experimental device is shown and the results are presented graphically. A more complicated "multistory" nonlinear model was also constructed from the similar triplets to study theoretically unsteady phenomena in turbulence, e.g., transient processes when f undergoes step changes.

Pozdynin, V. D. Analysis of empirical distributions of flow velocity in the ocean. FAiO, no. 10, 1973, 1105-1110.

A statistical analysis is presented of the empirical distribution of the oceanic current vector V in terms of its zonal u and meridional v components. The study is based on data obtained from flow measurements with buoy instruments positioned in 1969 during the second cruise of the R/V "Dmitriy Mendeleyev". Typical empirical histograms of V, u, and v are shown with the superposed theoretical probability curves calculated with allowance for non-random fluctuations of V, u, and v over the measurement internal.

Calculations of the probability density functions φ_ϵ were based on the assumption that the random variable x is the sum of the independent random terms y_i and the non-random term C_s^t at a time t. The theoretical probability curves $\varphi_\epsilon^{(V)}$ vs. V and $\varphi_\epsilon^{(v)}$ vs. v thus calculated are shown to be in good agreement with the empirical histograms. A physical interpretation of the statistical data is given, and the statistical dispersion of the instrument readings is evaluated. It is concluded from the analysis that a fairly objective breakdown of the analyzed process into two components is possible. The first component is determined by random small scale fluctuations and the second is a non-random component.

Preobrazhenskiy, L. Yu. Estimating components of turbulent energy balance in the surface boundary layer over water, from experimental data. IN: Tr. Gl. geofiz. observ., no. 297, 1973, 41-50. (RZhGeofiz, 12/73, no. 12B384)

The input-output turbulent energy balance at the sea surface-atmosphere interface is calculated, using experimental data on wind speed fluctuations at 2 to 3 levels above the surface; wave measurement data; and data on wind speed and air temperature gradients in the atmospheric boundary layer. The cited data were obtained by the author in 1965 in the North Atlantic and by B. M. Andreyev et al. in 1967 in the Baltic Sea. The approximated values of the components of energy balance and the input-to-output energy ratio are tabulated for both sets of experimental data. The average discrepancy between the input and output components of the energy balance is shown to be less than 50%. Under a stationary regime and a nearly neutral thermal stratification, conversion of wind energy into turbulent energy and dissipation of the latter in the form of heat were found to be the most significant components of turbulent energy balance.

The experimental evaluation data on the components of turbulent energy balance are compared with theoretical data obtained by solving a nonlinear set of equations which describe the structure of the atmospheric boundary layer over the sea. Agreement between the two sets of data is tolerably good.

Shevtsov, V. R., and A. P. Volkov. Method of studying the vertical structure of ocean currents from a drifting ship. Okeanologiya, no. 6, 1973, 1108-1113.

The procedure and equipment used by the authors for a continuous sounding of sea currents from a drifting ship are described, and

some sounding data are evaluated. Vertical profiles of current velocity and direction were obtained during the expeditions of the R/V "Dmitriy Mendeleyev" in the Indian Ocean near the equator. The equipment, designed at the Pacific Institute of Oceanography imeni P. P. Shirshov, AS USSR, consists of a two-coordinate Doppler shift current velocity meter and an analogue current direction meter which gives direction with respect to the magnetic meridian. The acoustic current meter, which is schematically described, measures Doppler shift Δf and hence current velocity vector v at a total estimated error $\Delta V = 0.5\%$, if the sound velocity value is accurate to $\pm$ 5 m/sec. This high accuracy makes it possible to study fluctuation phenomena. The analogue meter measures azimuth accurate to 3 deg. The combination of the two instruments and a depth sensor is designed for a maximum 2,000 m depth.

Typical vertical profiles of azimuth and v show that the measurements are most adversely affected by the rolling and pitching motion of the ship (down to 30 m depth) and the surface waves, respectively. The relative measurement data can be converted to absolute values, if drift of the ship is known. Various methods of drift measurement are outlined.

Vasil'yev, O. F., and V. L. Kvon. Investigation of stratified flows. IN: Gidrotekhn. str-vo, no. 8, 1973, 48-51. (RZhMekh, 12/73, no. 12B458). (Translation)

This paper gives information on the International Symposium on Stratified Flow (August 29-31, 1972, Novosibirsk), including classification and a brief review of the lectures, papers, and communications.

Zaslavskiy, M. M., S. A. Kitaygorodskiy, and L. G. Lobysheva. A linear model for the spatial spectrum of surface gravity waves generated by wind. FAiO, no. 10, 1973, 1077-1087.

The Phillips-Miles linear model of surface gravity waves generated by wind is developed into a closed set of equations, from which explicit analytical formulas are derived to describe statistical characteristics of a turbulent sea surface by means of a single parameter: the drag velocity v_* of the turbulent atmospheric boundary layer. The explicit formulas of the spatial spectrum $\psi(k, v_*, t)$ of surface waves and the coefficient of interaction $M(k)$ are given. Limitations to applications of the linear model of the surface waves interaction with a turbulent boundary layer are discussed.

The limitations to a qualitative description of the wind wave spectrum within wind speeds up to 30 cm/sec are imposed by the assumption of a weakly-quenched turbulence and the condition

$$k > k_i^o = \Omega / Z^o, \quad \Omega = 1 \tag{1}$$

where k^o and Z^o are respectively, the two-dimensional wave vector and the vertical coordinate (height of the boundary layer), and Ω is an empirical constant. Typical examples of the theoretical $\psi(k, v_*, t)$ spectra computed for given k, v_*, t, and angle θ values, show the main features of their formation and evolution.

Zhigulev, V. N. On the problem of propagation of disturbances in turbulent flows. IN: Sb. Chisl. metody mekh. splosh. sredy, v. 4, no. 2, 1973 51-61 (RZhMekh. 12/73, no. 12B850).

The problem of the linear stability of particular turbulent states is formulated in the case for which only the correlation functions of order less than n have non-zero values. In this case, the perturbation equations contain (n + 1) correlation functions; hence the perturbation system remains closed, although its order increases. A Fourier transform is then applied to derive a dispersion equation by a standard procedure.

Netyukhaylo, A. P., I. A. Sherenkov, A. I. Kobzar', V. M. Kuz'menko, and E. D. Telezhkin. Balance of turbulent energy in the boundary layer between fluids with different density. Vodosnabzh., kanaliz, gidrotekhn. sooruzh. Resp. mezhved. nauch. - tekhn. sb. no. 16, 1973, 87-92. (RZhMekh, 12/73, no. 12B853).

Reynolds stress equations and the Rott approximation are used to describe turbulence at the boundary between fluids with different density. Temperature pulsations which induce Archimedean forces are analyzed, disregarding density pulsations. Some earlier published experimental data (Netyukhaylo and Sherenkov, IVUZ Energetika, no. 4, 1969, 99-105; RZhMekh, 10/1969, no. 10B607) are used to plot distributions of different terms in the turbulent energy equation.

Belyayev, V. S., M. M. Lyubimtsev, and R. V. Ozmidov. On kinetic energy and temperature dissipation rate in the ocean. FAiO no. 11, 1973, 1179-1185.

Oceanic flow velocity and temperature fluctuation data, measured during the ninth cruise of the R/V "Akademik Kurchatov" in the Atlantic, are used to evaluate statistical properties of small-scale turbulence in the ocean. Measurement procedures and statistical treatment of the data are outlined briefly. The mean dissipation rates $\bar{\epsilon}$ and $\bar{N}$ of turbulent energy and temperature inhomogeneity are calculated at water depths to 140 m for two oceanic polygons with different hydrological conditions.

Calculations of $\bar{\epsilon}$ and $\bar{N}$ were made by two or more methods. The $\bar{\epsilon}$ and $\bar{N}$ values thus calculated, the mean square deviations $\bar{\sigma}_{\epsilon}$ and $\bar{\sigma}_{N}$ from the mean ϵ and $\bar{N}$, and the universal constant μ in the Kolmogorov theory of locally isotropic turbulence, are all tabulated for different water depths. The μ values were determined from the slope of the spectral curve of squared downstream velocity derivative in the inertial interval. The average μ value was calculated to be 0.56 ± 0.11. Occurrence of a pronounced intermittence in oceanic turbulence is concluded from comparison of the $\bar{\sigma}_{\epsilon}$ and $\bar{\sigma}_{N}$ data obtained by the authors and similar Western data obtained in a strait with tidal flow as well as in the open ocean.

Gorbatov, Yu. I., and A. A. Pivovarov. On the theory of T, S analysis of water masses under intensive turbulence exchange in the ocean. IN: Sb. Kompleks. issled prirody okeana. Mosk. un-t, no. 4, 1973, 101-110. (RZhMekh, 11/73, no. 11B474).

The problem is analyzed of vertical mixing and conversion of three water masses, two of them unbounded in the vertical direction and the third interposed with a finite depth 2 h. The coefficient of vertical turbulent thermal conductivity within each layer is considered to be constant and equal to the coefficient of salt diffusion. The cited coefficients are different for each water mass. The formulated problem is to some extent a generalization of the data obtained by V. B. Shtokman from a theoretical analysis of T, S curves (Selected works on marine physics. Moscow, Gidrometeoizdat, 1970, 18-64). Formalistic solutions for temperature and salinity distributions within each layer are obtained by solving standard Fourier linear differential equations, with allowance for the equalizing processes of vertical thermal conductivity and diffusion only. Conversions due to mixing of the water masses are studied in the T, S plane, and the geometry of the T, S curves thus obtained is examined.

Ivanov, Yu. A., and Ye. G. Morozov. A temperature variation analysis of the upper ocean layer. FAiO, no. 10, 1973, 1069-1076.

A statistical analysis is presented of temperature and current velocity data measured at depths to 250 meters in different regions of the Atlantic during the 5th and 9th cruises of the R/V "Akademik Kurchatov". Statistical functions which are discussed describe temperature and current velocity fluctuations within the frequency range of internal gravitational waves (from 10 min to 3 h). Vertical profiles of the frequency, current

velocity, and mean square temperature fluctuations are shown. The calculated statistical functions are plotted and their physical interpretation is given.

According to this interpretation, two types of fluctuations are distinguished by their mean square magnitude: the fluctuations determined by turbulence and those determined by internal wave processes. In contrast to the Phillips hypothesis, in all regions and at all times the same regularity was observed in all measurement data; the greater the data dispersion, the greater is the vertical correlation between fluctuation characteristics. In other words, internal waves do not degenerate into turbulence.

Filonov, A. Ye. Internal waves and present concepts of their effect on oceanographic investigation of certain physical fields in the ocean. Kompleksnyye issledovaniya prirody okeana, no. 4, 1973, 70-82. (RZhGeofiz, 12/73, no. 12V70)

A brief review is given of Soviet and foreign publications on the theory of origination and space-time variations in characteristics of internal waves, as well as their effect on certain physical characteristics of the ocean. Discussions are outlined on the future development and coordination of various scientific disciplines relating to internal waves.

Rusin, I. N. On a method for calculating the thickness of a quasihomogeneous oceanic layer. IN: Tr. Gl. geofiz. observ, no. 315, 1973, 123-138. (RZhGeofiz, 1/74, no. 1V52.1)

The model was considered of a quasistationary oceanic layer based on the equations of dynamics and thermoconductivity integrated over the entire layer thickness (V. I. Belyayev, V. F. Shapkina, 1967). The model assumes nonlinear conditions to apply at the lower boundary of the layer in question. Procedural data and some results of numerical experiments with the model are given for the case of no oceanic current. It is shown that in an annual evolution of the thickness of the quasihomogeneous layer three phases are distinguished: shallowing, stabilization, and deepening. For the North Atlantic the question was also considered of the dependence of layer thickness variation on the energy sources on the oceanic surface, for each of the indicated phases.

Girgidov, A. D. Tw- approaches to a description of turbulent diffusion. IN: Gidravlika i gidrotekhnika. Resp. mezhved. nauch. -tekhn. sb., no. 17, 1973, 9-14. (RZhMekh, 1/74, no. 1B1024)

Principal assumptions in the derivation of an equation for turbulent diffusion are considered, and advantages are suggested of another approach in which a finite velocity of diffusing particles is assumed. It is shown that the equation of diffusion with a finite velocity in two- and three-dimensional space is a particular case of the Kolmogorov equation. Using a specific example, the author makes a comparison between the solution obtained using the derived equation and that of the ordinary semiempirical parabolic equation of turbulent diffusion.

Konyayev, K. V., and K. D. Sabinin. Resonance hypothesis of internal wave generation in the sea. DAN SSSR, v. 210, no. 6, 1973, 1342-1345. (RZhGeofiz., 10/73, 1973, no. 10V63).

A resonance hypothesis of high-frequency internal wave formation in the ocean is introduced, to explain peculiar characteristics of internal wave trains observed by the authors in the Black Sea (DAN SSSR, v. 209, no. 1, 1973, 86) and by Western scientists in the tropical Atlantic. The earlier proposed mechanisms of internal wave generation give unsatisfactory explanations of some observed facts.

The resonance hypothesis postulates the existence of a nonuniform density distribution along a thermocline as an effect of internal waves. Oscillations from internal waves cause vertical contraction and expansion of the thermocline. A zone of isopyc contraction bounded on both ends by the expansion zones then forms a volume resonator for high-frequency internal waves. Horizontal nonuniformity of the thermocline is evidenced by peaks separated by troughs in the depth-horizontal coordinate plane. Resonators may form at the peaks, if the oscillation wavelength is a multiple of the resonator length. Oscillations in resonators may also be generated by shear instability owing to orbital motion of internal waves.

Evaluation of measurement data in the Atlantic and the Black Sea led to the assumption of the existence of closed resonance regions of high-frequency internal waves, possibly in the presence of low-frequency standing waves within a thermocline. Analysis of the internal wave spectra obtained from measurements in theCaspian Sea in 1972 revealed standing waves with non-zero coefficients up to 1.

Ivanov, A. P., and I. I. Kalinin. Determining optical characteristics of ocean waters by the laser sounding method. IN: Mor. gidrofiz. issled. Sevastopol', no. 1, 1973, 189-199. (RZhGeofiz, 12/73, no. 12V151) (Translation).

A procedure is described for determination of light attenuation ϵ and absorption k by sea water, from dispersion of reflected pulsed signal. A neodymium laser with power of 100 kw and pulse duration of 25 nsec (λ = 530 mm) was used. The back-scattered pulse was registered by an OF-233 objective with a diameter of 84 mm and photomultiplier FEU-36. Recorded signals were monitored by an SI-77 oscillograph. The experimental configuration was different for the measurements of ϵ and k. The effect of the pulse from the water surface on the measurement of k was investigated. Values of k were given as measured by the method described during the 26th trip of the scientific research ship "Mikhail Lomonosov".

Avaliani, D. I., and L. L. Kutateladze. Interaction of light with a turbulent fluid flow. ZhPMTF, no. 4, 1973, 115-123.

A theoretical correlation is established between mean square fluctuations $\langle n'n' \rangle$ of the index of refraction in a turbulent fluid flow, e.g., the ocean, and the mean flow rate fluctuations $\langle u \rangle$ at temperature T = const. The correlation is confirmed by experimental determination of the apparent increase Δn_T in n in turbulent distilled water at 293° K and different mean flow rates $\langle u \rangle$. The interferometric measurement of n is described and the experimental data are given as a $\Delta n_T = f(K^*)$ plot, where

$$K^* = (n^2 - 1) M^2 [(n^2 + 2)^2 C_1]^{1/3} \quad (1)$$

M is the Mach number, and C_f is the coefficient of friction.

The theoretical criterion

$$\tilde{K}_\lambda^T = \nu K_\lambda^T / \langle u \rangle \qquad (2)$$

of the turbulence effect on the laser beam attenuation factor K_λ^T in different liquids with different kinematic viscosity ν was studied experimentally. In theexperiments, K_λ^T was determined by measuring laser beam intensities I_1 and I_2 transmitted by a stationary liquid and the same liquid pumped through a tube at different flow rates. The characteristics of the experimental tubes and the lasers are tabulated. The experimental K_λ^T versus $\langle u \rangle$ plots for different tube diameters and different liquid parameters show a significant effect of turbulence on laser beam attenuation. The effect of laser beam λ (0.51 or 0.63 μ) was not observed. Dispersion of I fluctuations was found to increase with the increase in $\langle u \rangle$ and to decrease to a constant value with an increase in the aperture diameter of the receiver. Additional experimental data are also given on the broadening of the laser beam as a function of M.

Gurvich, A. S., and N. S. Time. Using a laser to evaluate the high frequency portion of a turbulence spectrum. MZhiG, no. 6, 1973, 142-145.

An experimental study of turbulence is described to determine the microstructure of a temperature field in a turbulent medium, using a method introduced by Gurvich. The method, claimed to be highly sensitive and simple, consists of measuring the frequency spectra of the logarithm of transmitted radiation intensity fluctuations and its derivative ΩU, where Ω is dimensionless frequency. A He-Ne laser (λ = 0.63 μ) was used as radiation source on a horizontal 50 m long path at 1 meter elevation above a flat bottom

surface. Reliable spectral density measurements were feasible at frequencies to 3.5 kHz.

Three experimental ΩU (Ω) spectra are shown to coincide with the theoretical spectrum model described by the function $\Phi_i(\varkappa\eta_k)$ of the refractive index $\varkappa$, which was derived from an asymptotic formula of Keller and Yaglom (MZhiG, no. 3, 1970). Coincidence of the experimental and theoretical data was best at $\sigma = 2$, where σ is the mean square logarithm of kinetic energy dissipation rate. Two other theoretical spectrum models coincide to a lesser degree with the experimental data obtained in this study. Since the formulas is question are asymptotic, the authors suggest further tests at higher frequencies in order to substantiate the proposed relationships.

Ivanov, A. P., and V. Ye. Shemshura. Method of evaluating absorptive index of light in the sea. IN: Sb. Mor. gidrofiz. issled. Sevastopol' no. 1 (60) 1973, 110-118. (RZhGeofiz, 12/73, no. 12V89). (Translation).

The approximate formula $k = 0.81\,\nu_{0,1}$ is introduced to determine the absorption coefficient k in sea water where $\nu_{0,1}$ is the vertical attenuation factor for half-space irradiance from above. The error of k determination is estimated to be 15-20%. The k values for different areas of the world ocean are calculated using literature data of different authors; the vertical attenuation factor ν_1 for horizontal irradiance from above was used instead of $\nu_{0,1}$.

Karabashev, G. L., and A. N. Solov'yev. Photoluminescence of sea water as an indicator of dynamic processes in the ocean. Okeanologiya, no. 4, 1973, 597-601. (RZhGeofiz, 12/73, no. 12V88).

Fluorimetric measurements of the spatial distribution of sea water photoluminescence in the area of the Atlantic boundary currents are reported and interpreted. The measurements were carried out at depths to 350 m in the western Sargasso Sea during the 12th cruise of the "Akademik Kurchatov" in March and April, 1972. The vertical profiles of seawater photoluminescence intensity and intensity distribution at 10, 100, and 200 m levels are mapped. The maps, together with simultaneously obtained standard hydrological observation data, show that intensity of sea-water luminescence can be used effectively as an indicator of dynamic processes in the active sea layer. This is made possible by a combination of several factors: a very high stability of luminescent organic compounds (the average lifetime of some bioluminophors is 1000 years); a vertical spread of 4 to 5 times in peak and average luminescence intensity in a given active layer of open ocean, and an even wider spread from area to area; and specific sensitivity of the measuring instrument to the "yellow matter" of the sea, provided that the selection of spectral parameters is right. The measured luminescence intensity value reacts by changing its first or second significant figure at even a fairly insignificant change in the structure of the medium.

Shevtsov, V. P. On calculation of the time structure of acoustic signals propagating in the ocean. IN: Sb. Fiz. metody issled. okeana. Vladivostok, 1973, 48-58. (RZhGeofiz, 12/73, no. 12V95). (Translation).

Reception sequence is described for different signal beams propagating in an underwater sound channel. Calculations and analytical expression of propagation characteristics are shown. Two cases are

discussed, when, for a given sound velocity vertical profile (SVVP), the function of distance does not exhibit extremums or positive or negative first derivative of the distance. It is shown that pseudocaustics corresponding to the minimum or the maximum of the function of distance may be obtained instead of the actual signal amplification, if the SVVP is approximated by linear functions. Any actual SVVP can be expressed by the Pedersen function and thus, continuity of the first derivative with respect to the ocean depth can be maintained. Several cases of pseudocaustics at the reception level are examined. Numerical data and the corresponding plots are given. It is concluded that better coincidence of data is obtained by the curvilinear segment approximation of SVVP rather than by substituting layers with a constant sound velocity gradient for the initial curve.

Kopelevich, O. V., and V. I. Burenkov. Statistical characteristics of optical scattering phase function by sea water. IN: Sb. Optika okeana i atmosfery. Leningrad, Izd-vo Nauka, 1972, 126-136. (RZhF, 6/73, no. 6D881). (Translation)

A statistical data analysis for three different areas of the World Ocean indicates that fluctuations of scattering are noticeably greater at large angles than at small angles. A strong correlation was detected between scattering for various angles within the 15-135° range, but only a weak correlation between scattering in the cited range and at small angles. The assumption is made that scattering at small and large angles is determined by coarse and fine independent fractions of marine suspensions. The position near 6° of the intersection of scattering phase functions may reflect the intersection in that range of the scattering phase functions for coarse and fine suspensions. The possibility is explored of expanding the experimental scattering phase functions into series of latent vectors of a covariant matrix.

Moroz, T. A. Correlation characteristics of sea reverberation from a sound scattering layer. IN: Tr. 4-y Vses. shkolyseminara po stat. gidroakustike. Novosibirsk, 1973, 84-92. (RZhF, 8/73, no. 8Zh634). (Translation).

Reverberation of sound from an inhomogeneous medium is analyzed under the assumption of sharp fluctuations of the scatterers' spatial distribution in an area with linear dimensions comparable to the distance a wave travels during one impulse. Relations are established between the emitted signal spectrum and the coherent or noncoherent scattered signals. The time-dependent reverberation correlation function is expressed through the spatial correlation function of the layer refractive index. It is shown that the theorem of superposition is valid only in the case when the correlation radius of refractive index fluctuations in a sound-scattering layer is small in relation to the wave length. A numerical example of calculation of the reverberation correlation function is given.

Gulin, E. P. Coherence of the acoustic field for sound reflected from a disturbed sea surface. DAN SSSR, v. 212, no. 5, 1973, 1082-1085.

The results of the measurement of the coherence of sound reflected from a disturbed sea surface are described. The equipment employed measured quadrature signal components $B' = B \cos \varphi_0 + C \sin \varphi_0$ and $C' = C \cos \varphi_0 - B \sin \varphi_0$, where φ_0 is determined from the travel time of the acoustic signal. The coherence parameter ϵ was calculated using forumla

$$\epsilon = \frac{(\overline{B'})^2 + (\overline{C'})^2}{\overline{B'^2} + \overline{C'^2}} = \frac{(\overline{B})^2 + (\overline{C})^2}{\overline{B^2} + \overline{C^2}}. \qquad (1)$$

Acoustic signals were emitted at a depth of 50 m and detected at a distance of 300 m by a vertical array of hydrophones at a depth of Z = 100 m. The emitted signals had frequencies from 300 Hz to 10 kHz, a pulse duration of 30 msec, and a pulse repetition rate of 0.2 and 0.4 sec.

The empirical dependencies of the coherence parameter ϵ on frequency for different wave heights are shown in Fig. 1. Analysis showed that the errors introduced by the measuring equipment lead to a decrease in the coherence parameter not exceeding 5-10%.

The empirical and calculated dependencies of ϵ on the Rayleigh parameter Φ are shown in Fig. 2 ($\Phi = 2k \sin \psi\sigma$, where σ is the rms wave height, $k = 2\pi/\lambda$, λ = sound wavelength, ψ - grazing angle).

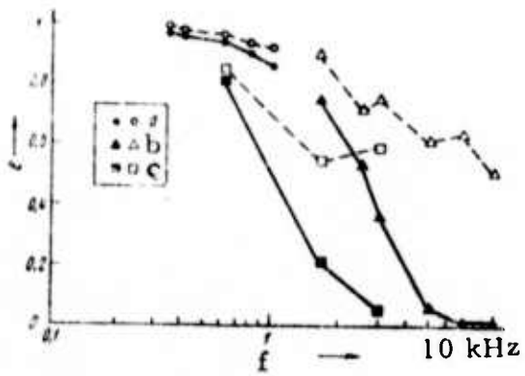

Fig. 1. Dependence of the coherence parameter on frequency for sea wave height σ = 6 cm (a), σ = 10 cm (b), σ = 23 cm (c).

Solid line - experimental curve; broken line - calculated.

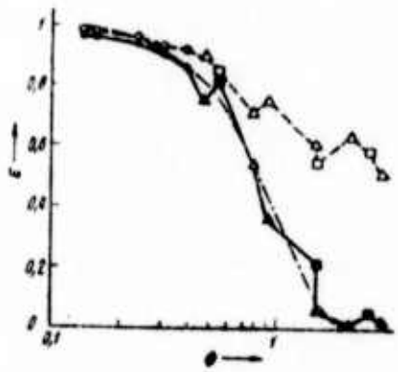

Fig. 2. Dependence of the coherence parameter on the Rayleigh parameter.

Dot-dash line - exp ($-\Phi^2$); a, b, c - same as Fig. 1.

The time and spatial coherence of acoustic signals reflected from the sea surface are illustrated in Figs. 3 and 4, respectively. The time coherence (see Fig. 3) decays with an increase of Δt to a level d determined by ϵ at all frequencies. The coherence time for the fluctuating

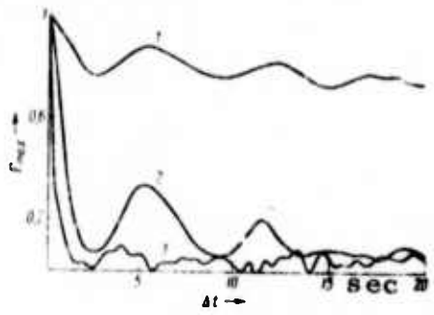

Fig. 3. Degree of the time coherence for f = 0.6 kHz, Φ = 0.55 (1), f = 1.5 kHz, Φ = 1.3 (2), f = 3 kHz, Φ = 2.7 (3).

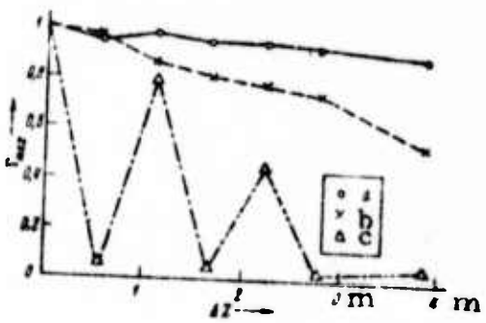

Fig. 4. Degree of the spatial coherence for f = 0.6 kHz (a), f = 1.5 kHz (b), f = 3 kHz (c).

component of the acoustic field was fund to be 1, 0.8 and 0.4 sec at frequencies of 0.6, 1.5 and 3 kHz, respectively.

The spatial coherence depends on frequency (see Fig. 4). The degree of the spatial coherence Γ_{max} at ΔZ_{max} = 4 m was found to be 0.9, 0.55 and 0.05 at frequencies of 0.6, 1.5 and 3 kHz, respectively. The steady level of coherence for large ΔZ was calculated to be 0.7, 0.1 and 0.02 at frequencies of 0.6, 1.5 and 3 kHz, respectively.

Kogan, V. Ya. Possibility of using sound scattering phenomena in the sea for oceanographic measurements. IN: Sb. Fiz. metody issled. okeana. Vladivostok, 1973, 38-43. (RZhF, 11/73, no. 11Zh787), (Translation)

A theoretical quantitative evaluation is made of data from feasible experimental studies of inhomogeneous oceanic structure using methods based on the sound scattering theory. A possible solution to certain oceanological problems is described using a method based on the Khintchine-Wiener theorem.

Medvedev, S. N. Reproducing a velocity profile from data on the time structure of an acoustic signal. IN: Sb. Fiz. metody issled. okeana. Vladivostok, 1973, 15-18. (RZhGeofiz, 12/73, no. 12V94; RZhF, 11/73, no. 11Zh786). (Translation).

The problem is examined of reproducing a velocity profile from the known relation of the full-cycle beam length to the sound velocity at the turning point. The function D(v) is determined from the time structure data on the acoustic signal. There is an infinite number of solutions to the problem thus formulated. This solution ambiguity can be eliminated by additionally requiring knowledge of the sound velocity distribution above or below the channel axis. Then the velocity profile below or above the axis, respectively, is uniquely defined. The accuracy of this method of reproducing the vertical distribution function of sound velocity is analyzed.

Fizicheskiye metody issledovaniya okeana.
(Physical methods of studying the ocean).
Vladivostok, 1973, 93 p. (RZhGeofiz, 12/73,
no. 12V13 K). (Translation)

This is a collection of 13 articles relating to problems of using acoustic, optical and other physical methods of studying the ocean. Problems of establishing the vertical distribution of sound velocity are considered, based on the results of time and angular characteristics of acoustic fields. Oceanographic investigation methods are generally discussed in terms of measurements of acoustic field parameters. Experience in using devices based on acoustic principles is summarized. Results are described of experimental studies on propagation of UV radiation in seawater. Prospects and ways are presented for the practical use of NMR methods in oceanographic measurements. Several papers consider theoretical methods for evaluating transmissibility conditions of acoustic signals in the ocean.

Ostrovskiy, L. A., and Ye. N. Pelinovskiy. Nonlinear waves in an inhomogeneous dissipative medium. IN: Prob. difrakts. i rasprostr. voln, 12/73, no. 44-51.

Wave profile transformations resulting from inhomogeneity and energy dissipation in the medium are studied theoretically. The wave profile is determined by the form of the function $\partial Z/\partial\theta$, where Z is the Jacobian and θ is the wave phase. The wave profile $\partial Z/\partial\theta$ is plotted for different values of γ, the parameter of the wave non-sinusoidality (Fig. 1). At a small γ the wave profile is nearly sinusoidal, or $\partial Z/\partial\theta \sim \gamma\cos\theta$. At $\gamma = 1$ the wave is solitary (soliton), or $\partial Z/\partial\theta \sim \mathrm{sech}^2\theta$. Both wave systems

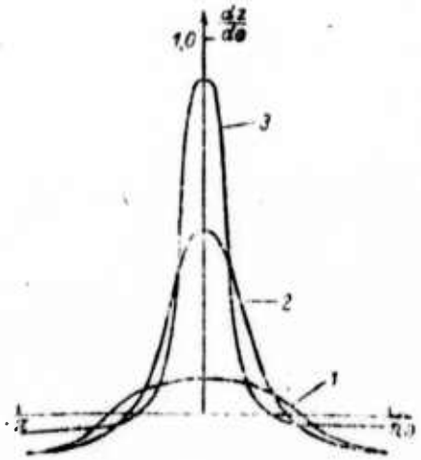

Fig. 1. Wave profiles at three different γ values in the absence of dissipation.

are described by the Korteweg-de Vries equation. Generally, this equation is not applicable to inhomogeneous systems with energy dissipation, but at small dissipation parameters α and δ and a smooth velocity evolution c(x), a wave can be considered as nearly cnoidal.

Propagation of nonsinusoidal waves in a dissipative medium is described by a set of partial differential equations containing Lagrangian L and Rayleigh R functions. A solution to the boundary value problem at a given point x = with wave amplitude A_c, wave number k_o, frequency ω_o, and γ_o is presented in the form of the single equation

$$\frac{d}{dx}[c^9 Y_1(\gamma)] = -2\alpha c^8 Y_1(\gamma) - 2\delta\omega^2 c^6 Y_2(\gamma), \qquad (1),$$

where $Y_1(\gamma) = K^2\langle Z_\theta{}^2\rangle$ and $Y_2(\gamma) = K^2\langle Z^2{}_{\theta\theta}\rangle$. Solution of (1) for γ is obtained in the cases of a nearly harmonic wave ($\gamma \leq 1$) and a train of weakly interrelated solitons ($1 - \gamma \leq 1$). In the latter case, at $\alpha = 0$, i.e., in the absence of friction, and c = const, amplitude A of a soliton is independent of boundary conditions at $x \to \infty$.

At $\delta = 0$, i.e. in an inviscid liquid, and c = const, soliton amplitude decreases exponentially, but the exponent is greater than in the A expression for a harmonic wave. At $\alpha = \delta = 0$, γ increases with decrease in c(x), and hence a wave is transformed into a train of solitons C$\gamma \geq 0.95$. In this case the formula $C^9(x)\, Y_1(\gamma) = \text{const}$. describes the actual wave transformation on a liquid surface. In a homogeneous medium, energy dissipation is described by the absorption coefficient which varies significantly near $\gamma = 1$ only. In this case, a quasilinear approximation of the wave is applicable.

The cited theoretical conclusions are found to be in good agreement with experimental data for water waves and nonlinear r-f waves in transmission lines.

Berkovskiy, B. M., and A. K. Sinitsyn. Thermoconvection waves in a layer with free boundaries. I-FZh, v. 26, no. 1, 1974, 104-111.

A mathematical model for thermal convection waves propagating in a thin fluid layer of finite thickness (order of 1 cm) is developed to determine the effect of free horizontal boundaries on propagation of slowly decaying waves. The authors assume that a vertical temperature gradient γ is maintained constant by heating the bottom boundary and the fluid expands, if γ is made parallel to gravity force g. Thermal convection waves are generated from a source of periodic disturbances over a vertical boundary of the semi-finite horizontal fluid layer.

There is a threshold γ_c above which thermal convection waves become unstable. The γ_c value is determined by fluid layer properties and the boundary value characteristics of periodic disturbances. Propagation below and above γ_c of thermal convection waves of small amplitude in a Newtonian and a viscoelastic fluid is described by sets of linear partial differential equations. Solution of these equations makes it possible to compute wave characteristics as functions of the Rayleigh number R of fluid flow between two horizontal free planes.

The logarithmic decrement $\delta = 2\pi k_2/k_1$ of convection waves, where k_1 and k_2 are the components of wave vector k, is found to depend on the fluctuation frequency ω, the Prandtl number Pr, the Grashof number Gr, and in a viscoelastic fluid, on the characteristic relaxation time τ. Numerical values of δ, group velocity U_{gr}, and wavelength λ are plotted against R for different ω, Pr = 1 or 10, and for a viscoelastic fluid, τ = 0.6 and 0.5. Analysis of the theoretical $\delta^{1/2}$ vs. R plots (Fig. 1) shows that decay of all convection waves slows down (δ decreases) in the presence of a negative γ across a Newtonian fluid layer. The slowdown is significant

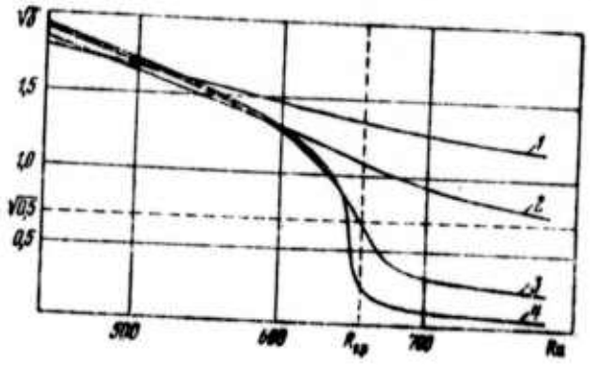

Fig. 1. Logarithime decrement versus R (Pr = 1) in a Newtonian fluid. Curves 1, 2, 3, and 4 denote ω = 3, 1, 0.1 and 0.01, respectively.

for the low-ω waves at $R \geq R_{cr}$ and simultaneous with a sharp increase in U_{gr}. That the free boundaries have a significant effect on wave propagation is shown by λ variations within 2-3 range of layer thickness h.

The authors conclude that propagation of slow decaying convective waves in a thin layer of a Newtonian fluid is possible for the case of $\gamma \parallel g$, but only in the vicinity of or above the mechanical stability threshold. Analysis of the analogous theoretical data for a viscoelastic fluid layer reveals the possible existence of slowly decaying convective waves of two types: in the vicinity of a monotonic instability threshold R_M, and in the vicinity of an oscillatory instability threshold, $R_{k1} < R_M$ or $R_{k2} \geq R_M$, depending on ω of the waves. The R-dependence of the wave λ and U_{gr} of low-ω slowly decaying waves is similar to that in an ordinary Newtonian fluid.

Berezin, Yu. A. On numerical solutions to the Korteweg-de Vries equations. IN: Chisl. metody mekh. splosh. sredy, Novosibirsk, v. 4, no. 2, 1973, 20-31. (RZhMekh, 1/74, no. 1B576).

The Korteweg-de Vries equation is the model equation for describing waves with a small but definite amplitude in dispersive media. In the general case, integration of this equation is possible only by numerical methods, although in a number of cases an analytic solution in closed form can be obtained under certain particular initial conditions. This fact is used by the author for comparing the effectiveness of various difference schemes for numerical solution to the Korteweg-de Vries equation. Such a comparison resulted in the examination of the three conservation laws, position and amplitude of extended waves for an approximate solution, as well as in the calculation of the standard deviation of an approximate solution. Five difference schemes were considered.

Criteria for the calculation rigorousness were given for all schemes. The article includes numerous critical comments on the results obtained by other authors in the USSR and abroad.

Dotsenko, S. F., and L. V. Cherkesov. Effect of a continuous change in fluid density on waves generated by moving surface presseres. MZhiG, no. 6, 1973, 55-62.

This article contains the formulation and solution by linear approximation of the problem of developed internal waves in an ideal incompressible fluid with nonuniform density. The wave generator is a

local surface pressure moving at a constant velocity, analogous to the action of a cyclone moving over the ocean surface. The hydrodynamic model is developed as follows.

A basin $-H \leq z \leq 0$, which is a part of the space $-\infty < x < +\infty$ is assumed filled with an incompressible fluid. The fluid density in its undisturbed state is a continuous function of z. Pressure is applied to the free surface of the fluid, represented by

$$p_0 = af(x+vt) \qquad (v>0) \tag{1}$$

where a, v are constants, and f (ξ) is an even function that is zero at $|\xi| > \ell$.

In the linear formulation (in variables $x_1 = x + vt$, z), the problem of the effect on the internal waves generated by the pressure (Eq. 1) of a continuously changing density along the z-axis reduces to the solution of the following boundary value problem:

$$\begin{aligned} &vu_x = -\rho_0^{-1}(p_x + p_{ax}),\ vw_x = -\rho_0^{-1}g\rho - \rho_0^{-1}p_z \\ &u_x + w_z = 0, \quad v\rho_x + \rho_{0z}w = 0 \end{aligned} \tag{2}$$

$$p - \rho_1 g\zeta = 0, \quad v\zeta_x - w = 0 \quad (z=0), \quad w = 0 \quad (z=-H) \tag{3}$$

where u, w are the x and z components of the velocity vector; p, ρ = dynamic disturbances of pressure and density; ζ = deviation of the free surface from z = 0; $\rho = \rho_0$ (2) fluid density in its undisturbed state; and $\rho_1 = \rho_0$ (0) is a known constant.

On the assumption that $-H \leq z_2 \leq z_1 \leq 0_1$, $k > 0$ and

$$\rho_0(z) = \begin{cases} \rho_1, & z_1 \leq z \leq 0 \\ \rho_1 \exp k(z_1 - z), & z_2 \leq z \leq z_1 \\ \rho_1 \exp k(z_1 - z_2), & -H \leq z \leq z_2 \end{cases}$$

the solution of the boundary problem is found by use of Fourier transforms.

Finally, assuming $v_{n+1} < v < v_n$, the following expression is derived:

$$w=\theta(x)\sum_{i=1}^{n} w_i(z)\cos m_i x+w_0(x,z) \qquad (|x|>l) \tag{4}$$

$$w_i=-2\sqrt{2\pi}\alpha m_i f^*(m_i)\Delta_i(m_i,z)[\Delta'(m_i)]^{-1}$$

where w_o is an uneven function of x, exponentially tending to zero at $|x|\to\infty$, and θ is the Heaviside function. At $v > v_1$ continuous wave motion does not originate.

Then from the continuity equation and the foregoing equations, the expressionf for u(x, z) is derived in the following form

$$u=\theta(x)\sum_{i=1}^{n} u_i(z)\sin m_i x+u_0(x,z) \qquad (|x|>l,\ u_i=-m_i^{-1}w_{iz}) \tag{5}$$

where u_o is an even function of x, exponentially tending to zero at $|x|\to\infty$.

Thus behind a pressure surface moving at $v < v_1$ an internal wave wake is generated which is comprised of a finite sum of progressive waves propagating at phase velocity v.

In order to find a numerical solution for v_n $(n \geq 2)$ the parameter space is divided into G_n regions as shown in Fig. 1. In each region, continuous wave motion is comprised of n progressive waves. It

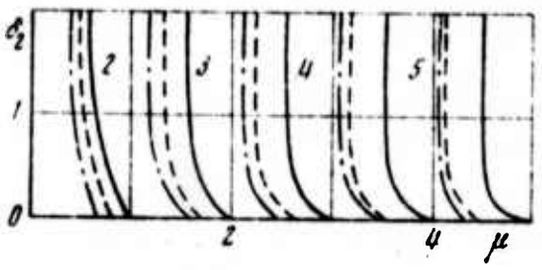

Fig. 1. $\mu = \sqrt{gh_2\epsilon}\,(\pi v)^{-1}$; $\epsilon = 10^{-2}$; $\delta_1 = 0,\ 0.2,\ 0.6$ (solid, dashed, dot-dash line, respectively)

was found that v_n increases with h_1 and h_3 (as illustrated by Fig. 2) as well as with h_2 and ϵ_1 and can be considered to be proportional to $\sqrt{\epsilon}$. Table 1 illustrates the dependence on $h_{1,\ 3}$ (m) and v_n (in sec^{-1}) for $\epsilon = 10^{-2}$ and $h_2 = 100$ m.

Table 1

h_1	h_3	v_1	v_2	v_3	v_4	v_5
0	$2 \cdot 10^2$	54.2	1.70	0.65	0.39	0.28
	$2 \cdot 10^3$	143	1.95	0.66	0.40	0.28
20	$2 \cdot 10^2$	56.0	1.99	0.76	0.45	0.31
	$2 \cdot 10^3$	144	2.32	0.77	0.45	0.31
10^2	$2 \cdot 10^2$	62.6	2.75	0.88	0.48	0.33
	$2 \cdot 10^3$	147	3.49	0.91	0.49	0.33
10^3	10^3	143	7.05	0.98	0.50	0.33

Fig. 2 shows the dependence on $\mu = \sqrt{gh_2\epsilon}\,(\pi\nu)^{-1}$ of the dimensionless wave numbe· $m_n^* = m_n h_2$ $(n \geq 2)$ $(\lambda = 2\pi m_n^{-1})$. The wavelength λ_n $(n \geq 2)$ decreases with an increase in h_1, h_3, ϵ and a decrease in ν, as illustrated in Fig. 2, as well as with an increase in h_2.

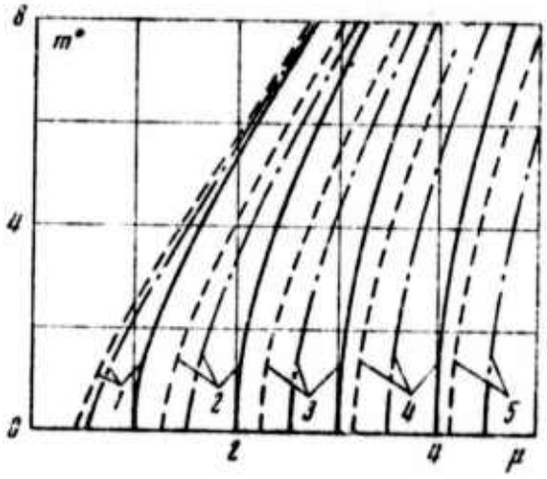

Fig. 2. $\epsilon = 10^{-2}$; $\delta_1 = \delta_2 = 0$ (solid line), $\delta_1 = 0$ and $\delta_2 = 10$ (dashed line), $\delta_1 = 0.2$ and $\delta_2 = 10$ (dot-dash line).

The dependence on z of the amplitude of individual waves is illustrated in Fig. 3.

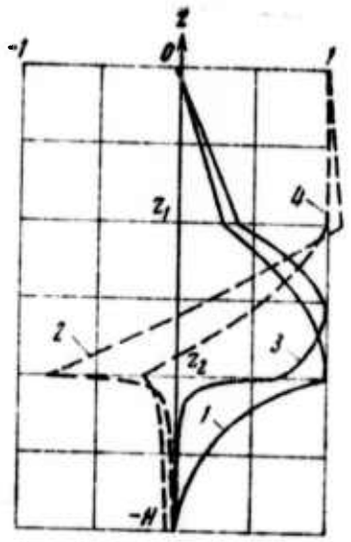

Fig. 3. w_2 (2) (1 and 3) and u_2 (2) (2 and 4)

$H = 2 \times 10^{-3}$ m; $h_1 = 20$ m; $h_2 = 100$ m; $\epsilon = 10^{-2}$. Analysis shows that waves with numbers $n \geq 2$ result from fluid heterogeneity and are typical internal waves. Their velocities reach extremes in the heterogeneous layer. An analysis of $A_n = \max |w_n(z)|$, $B_n = \max |u_n(z)|$ $(-H \leq z \leq 0)$ shows that: A_1 and B_1 are reached at $z = 0$; B_2 at $z = z_1$; and A_n, B_n $(n \geq 2)$ at $z_2 \leq z \leq z_1$. For internal waves, $\varphi_n = B_n A_n^{-1}$ $(n \geq 2)$ in the interval $(0, v_n)$ increases monotonically with v. The value $v = v_n$ is resonant for the n-th wave.

3. Unattenuated wave motion at a sufficient distance from the local pressure excitation is expressible as a finite sum of progressive waves of various lengths and amplitudes. Simplified calculations can be made with f(x) given in the form

$$f(x) = \cos[\pi x (2l)^{-1}] \quad (|x| < l), \quad f(x) = 0, \quad (|x| < l) \tag{6}$$

Additional expressions are introduced to estimate the contribution of each s-th internal wave to the wave motion. Results show that the greatest contribution to the wave motion is that of the longest wave (n-th at $v_{n+1} < v < v_n$). Analysis of the dependence of the wave motion on the thickness of the homogeneous layers shows that at $h_3 \times h_2 \geq 2.5$ the amplitude of the internal waves is practically independent of h_3, but strongly depends on h_1.

Zakharov, V. M., O. K. Kostko, A. I. German, V. I. Pavlov, and V. Ye. Rokotyan. Method of measuring the geometric characteristics of the roughness of water and other surfaces. Otkr izobr, no. 6, 1974, 111 (Author Certificate no. 415489).

A Soviet patent whose development was sponsored by the Central Aerological Observatory has been issued for a method of measuring the geometric characteristics of the roughness of water and other surfaces. The method uses optical pulses to sound the surface, with subsequent phase comparison of the emitted and reflected signal pulses. In order to improve accuracy, as well as measurement radius and reliability from a moving platform, the transmitted nanosecond optical sounding pulses have a beam width commensurate with the dimensions of roughnesses being measured. The reflected pulse width is compared with the sounding pulse width and, depending on the sounding angle, the height or length of the surface roughness is determined from the increase in duration of the reflected pulse.

Krasyuk, N. P., B. Sh. Lande, I. I. Megretskaya. Effect of radar resolution on the spectral width of a microwave signal scattered by the sea surface. RiE, no. 10, 1972, 2182-2184.

An analysis is made of the effect of the size of the resolution cross section on the spectral width of r-f waves scattered by a sea surface. An expression for the spectrum of scattered r-f waves is derived from the space-time correlation function, assuming a finite spectrum of large sea waves and a zero shift of the irradiated area center in the incidence plane.

The spectral width increment at the half-power level, derived from the envelope spectrum is determined to have the form

$$2\Delta f = \sqrt{2.8\beta + \delta^2} / \pi. \qquad (1)$$

where δ is attenuation constant for capillary waves, $\beta = 6.4\, v^2/x^2\, a_2^2\, \mathrm{erfc}\,(0.275\, L/v^2)$ in which v is wind velocity in m/sec, $\alpha = \sin\varphi$ (φ = incidence angle of r-f beam), and L is a linear dimension of the resolution cross section.

The results of the analysis are shown in Fig. 1. Results

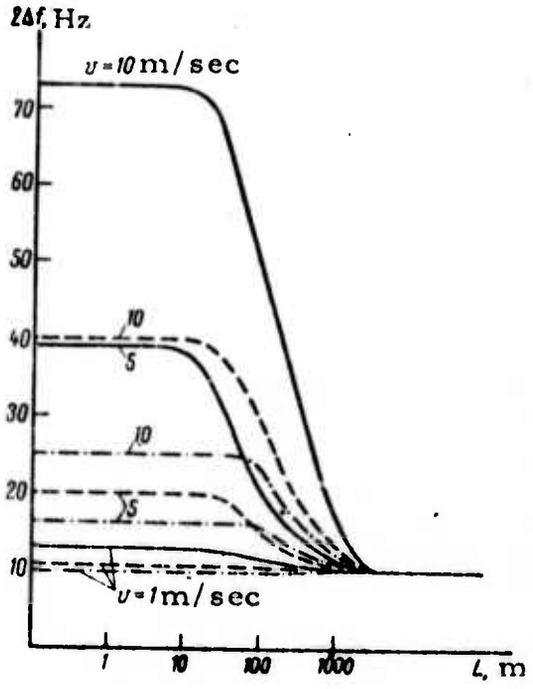

Fig. 1. Dependence of the spectral broadening on the linear dimension L of the resolution cross section.

Solid line - incidence angle measured from the horizontal = 10°;
dashed line - = 5°;
dot-dash line - = 3°.

indicate that under high resolution conditions the value of $2\Delta f$ increases with both wind velocity and beam incidence angle. The minimum incident angle under the assumed conditions is given as $3\text{-}4^{\circ}$.

Zhivotovskiy, L. A. Polarization state of signals reflected from a group of independently fluctuating targets. RiE, no. 10, 1972, 2184-2186.

A geometrical method is presented for determining polarization characteristics of the reflected superposed signals from a group of independently fluctuating targets. Noncorrelated, quasimonochromatic and partly polarized signals reflected from a group of two fluctuating targets are represented by

$$\begin{aligned} S_1 &= S_{1p} + S_{1u} \\ S_2 &= S_{2p} + S_{2u} \end{aligned} \tag{1}$$

where indices p and u denote polarized and unpolarized components. The components S_{1p} and S_{p2} are represented by points M_1 and M_2 on the Poincare' sphere as shown in Fig. 1. It follows from the coherence matrix that the

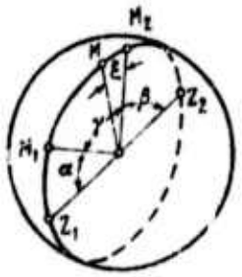

Fig. 1. Poincare' sphere.

polarized component of the summary wave $S_{\Sigma} = S_1 + S_2$ lies on the circle $Z_1 M_1 M_2 Z_2$ and is represented by point M. The position of $S_{\Sigma p}$ as determined

from the coherence matrix is given by

$$\xi = 90^\circ - \operatorname{arc\,tg}\left[\frac{k + \cos\gamma}{\sin\gamma}\right] \tag{2}$$

where $k = P_{2p}/P_{1p}$ is the ratio between power flux densities of polarized components of S_1 and S_2 waves. The degree of polarization of the summary wave is given by

$$p = \frac{P_{1u}(\sin\alpha + k\sin\beta)}{P_{1u}(1+k) + P_{1u} + P_{2u}}. \tag{3}$$

Plots of (k, ξ) and $p(k, \gamma)$ calculated by the given formulas for $P_{1u} = P_{2u} = 0$ are shown in Fig. 2.

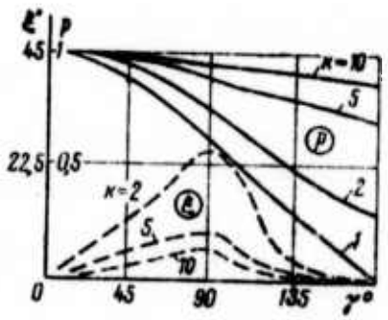

Fig. 2. ξ and P as functions of k and γ.

The polarization characteristic of the summary wave for the case where $n > 2$ can be determined by analogous geometrical constructions on the Poincare' sphere, as illustrated in Fig. 3 for $n = 3$ and $n = 6$.

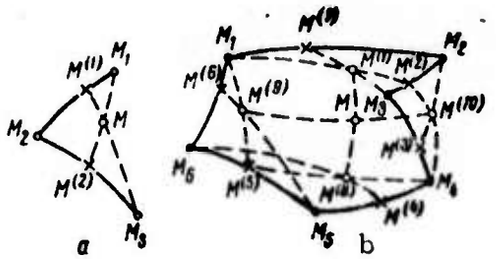

Fig. 3. Polarization of the summary wave for n = 3(a) and n = 6(b).

It thus follows that the position of any number of points n may be found from (2), and the net polarization is obtained by simple construction on the Poincare' sphere.

Babayev, A. B., I. A. Pavlova, and V. P. Prakhov. Patterns of reflection from a sea surface. IN: Tr. Mosk. energ. in-ta. Radiopriyemnyye ustroystva, no. 110, 1972, 77-79.

Patterns of backscatter from a sea surface were measured in different directions relative to sea wave crest line, at irradiation angles varying from $\alpha = 90^{\circ}$ to $\alpha = 10^{\circ}$, measured from the horizontal. A block diagram of the experiment is shown in Fig. 1. The parameters of the test equipment were: wavelength $\lambda_1 = 7$ cm, $\lambda_2 = 15$ cm; frequency deviation $2\Delta f_1 = 100$ MHz, $2\Delta f_2 = 8$ MHz; directional pattern width in both planes $\Delta\gamma_1 = \Delta\beta_1 = 6.5^{\circ}$, $\Delta\gamma_2 = \Delta\beta_2 = 10^{\circ}$. Both vertically and horizontally polarized incident waves were used.

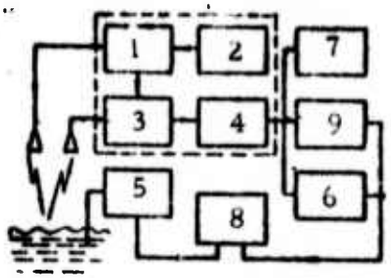

Fig. 1. Backscatter experiment

1- UHF generator; 2- modulator; 3- mixer; 4- amplifier; 5- voltmeter; 6- frequency meter; 7- tape recorder; 8- loop oscillograph; 9- wave meter.

The backscatter patterns at horizontal (λ = 15 cm) and vertical (λ= 7 cm) polarization are shown in Fig. 2 and Fig. 3 respectively.

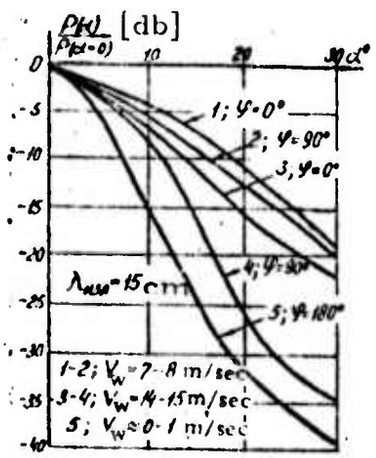

Fig. 2.

Backscatter pattern,
λ = 15 cm

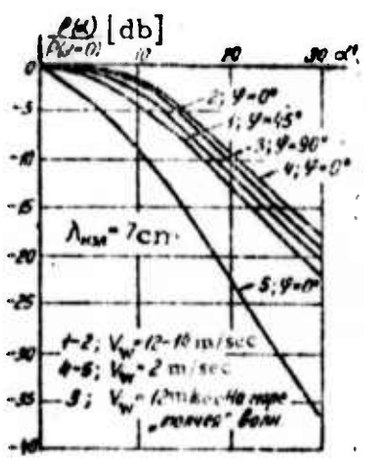

Fig. 3.

Backscatter pattern,
λ = 7 cm

$\varphi = 0^{\circ}$ - measuring plane perpendicular to the sea wave crestlive;
$\varphi = 90^{\circ}$ - parallel.

As seen in Figs. 1 and 2, the main lobes broaden with increase in wind velocity V_w.

It is concluded that backscatter patterns at the sea surface depend on the sea state and the direction of radiation relative to the sea wave propagation; however they have only a weak dependence on the transmitted wavelength.

Nedelyayev, A. M., V. P. Prakhov, and T. A. Osetrova. Determination of geometrical characteristics of the sea surface from a signal scattered by it. IN: Trudy Moskovskogo ordena Lenina energeticheskogo instituta. Radiopriyemnyye ustroystva, no. 110, 1972, 80-83.

The geometrical characteristics of a rough sea surface were determined using experimental data on radio waves scattered by it (Babayev et al., foregoing article) in two ways: a) by the Kirchhoff method applied to a composite rough surface (Beckman, 1965); and b) by the Kirchhoff method combined with perturbation theory (Fuks, IVUZ Radiofiz, no. 5, 1966).

Assuming that the distribution law and spatial autocorrelation function for heights of a rough sea are known, the authors describe scattering by

$$P_K(\theta) = f_1(\theta, a, b, c, d) \quad (1)$$

$$P_{KP}(\theta) = f_2(\theta, a, b, c, d) \quad (2)$$

where $P_K(\theta)$ is power scattered by a rough surface derived by the Kirchhoff method, $P_{KP}(\theta)$ is the same derived by the Kirchhoff plus perturbation method, θ is irradiation angle measured from the vertical, $a = \delta_{h1}$ and $b = \delta_{h2}$ are rms heights of large and small roughness (waves and ripples); and $c = \gamma_{h1}$ and

$d = \gamma_{h2}$ are rms slope angles of large and small roughness states.

The unknown parameters a, b, c, d are determined by the least-squares method from the experimental curve $P_E(\theta)$ as

$$\sum_{i=1}^{n} [P_E(\theta_i) - f_1(\theta_i, a, b, c, d)]^2 = \min; \tag{3}$$

and

$$\sum_{i=1}^{n} [P_E(\theta_i) - f_2(\theta_i; a, b, c, d)]^2 = \min. \tag{4}$$

$P_K(\theta)$ and $P_{KP}(\theta)$, calculated using parameters a, b, c, d (i.e. σ_{h1}, σ_{h2}, γ_{h1}, γ_{h2}) determined by (3) and (4), are shown in Figs. 1-3 together with the experimental curve $P_E(\theta)$ of Babayev et al.

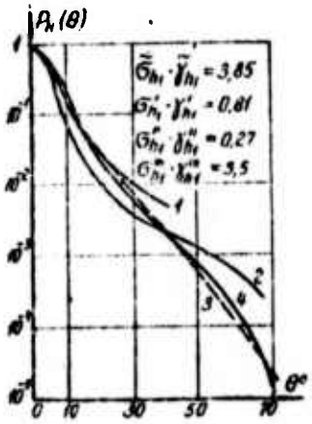

Fig. 1.

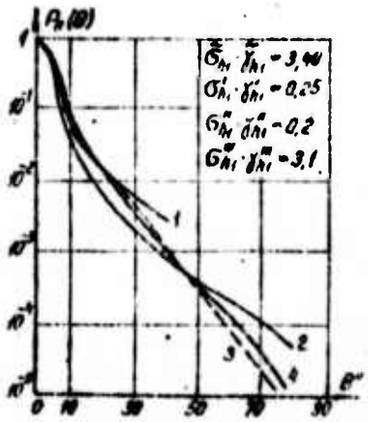

Fig. 2.

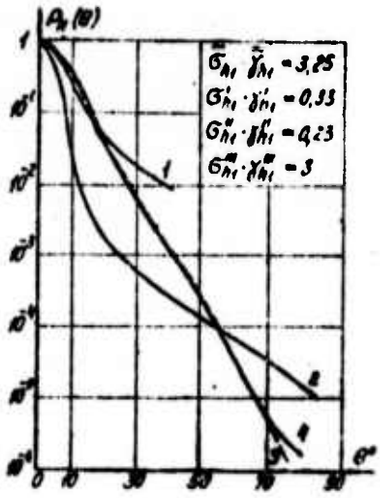

Fig. 3.

Fig. 1-3. Power scattering vs. angle.
1- $P_K(\theta)$ calculated from $\sigma'_{h1,2}$ and $\gamma'_{h1,2}$; 2- $P_K(\theta)$ from $\sigma''_{h1,2}$ and $\gamma''_{h1,2}$; 3- $P_{KP}(\theta)$ from $\sigma'''_{h1,2}$ and $\gamma'''_{h1,2}$; 4- experimental curve.

It is seen from the figures that curves 3 calculated by (2) are in good agreement with experimental dependence an irradiation angles of r-f power scattered by a sea surface. In addition, parameters $\bar{\sigma}_{h1}$ and $\bar{\gamma}_{h2}$ (see Figs. 1-3) measured by string wavegraph, agree well with those determined from Eq. (4).

The authors conclude that the Kirchhoff plus perturbation method is more acceptable than the Kirchhoff method alone, as applied to a composite rough surface for the description of r-f scattering by it.

Kalmykov, A. I., A. S. Kurekin, V. Yu. Levantovskiy, I. Ye. Ostrovskiy, and V. V. Pustovoytenko. Characteristics of radio signals, scattered by the sea surface in directions close to that of a mirror reflection. IVUZ Radiofiz, no. 10, 1973, 1498-1503.

Results are described of measurements of polarization, energy and spectral characteristics of r-f signals scattered by a sea surface. The experiments were carried out over two paths using linearly polarized waves at λ = 3.2 and 10 cm and highly directional antennas. The paths were parallel to the wave crestline. The geometry of the experiments are specified in Fig. 1 and Table 1.

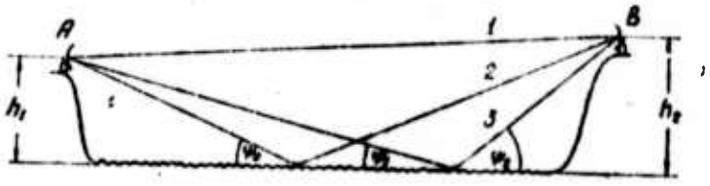

Fig. 1. Test configuration.

Table 1

Lay-out	h_1, м	h_2, м	R, км	ψ_0,	$\psi_{1\,min}$	$\psi_{2\,max}$	$\varphi_{A/B}$ (λ = 3,2 см),	$\varphi_{A/B}$ (λ = 10 см),
I	8	18	0,4	3,5	1,5	10	2 / 1	6 / 3
II	560	120	16,5	2,5	2,0	20,8	2 / 2	3 / 3

Note: R is path length; φ_A and φ_B are pattern widths at the half power points.

The dependences on glancing angle of the average level of scattered signals, normalized to the level of a direct signal, are shown in Fig. 2 and Fig. 3.

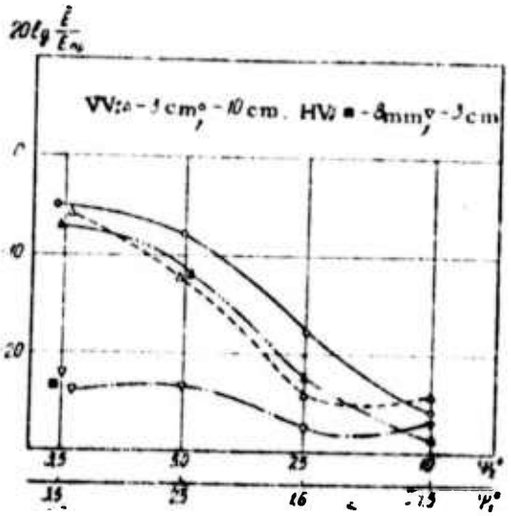

Fig. 2. The dependence on glancing angles of the normalized levels of mirror reflections and scattered signals.

VV- vertical polarization of emitted and detected waves; HV- horizontal polarization of emitted, vertical of detected waves. Open symbols indicate a smooth sea; solid - 1-2 ball.

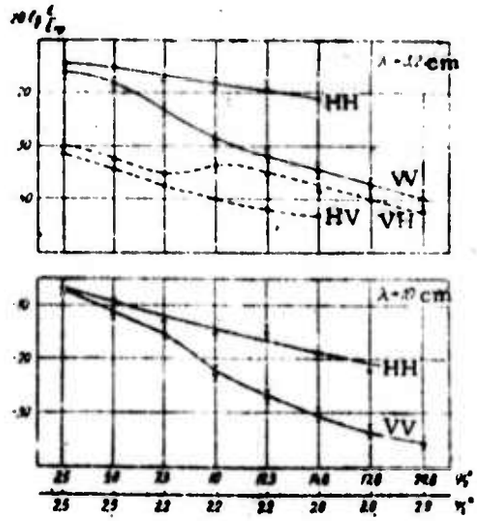

Fig. 3. Same as in Fig. 2, for path 2.

VV- bath emitted and detected signals vertically polarized; HH- horizontally; VH and HV- emitted and detected signals have different polarization.

An analysis of the results obtained for path 1 shows that the level of mirror reflections is lower than that of direct signals by 5-7 db in the case of a matched polarization of emitted and detected signals (VV), and by more than 20 db in the case of unmatched polarization (HV). The level of scattered signals drops rapidly with an increase in angle ψ_2. The results obtained for path 2 show that the levels of mirror reflections with both vertical and horizontal matched polarizations (VV and HH) are (-)15 db at λ = 3.2 cm and (-) 7 db at λ = 10 cm. The dependences on ψ_2 of scattered signals with matched polarizations are similar at λ = 3.2 cm and λ = 10 cm.

The depolarization for mirror reflections and scattered signals is shown in Fig. 4. As seen from Fig. 4, at horizontal polarization

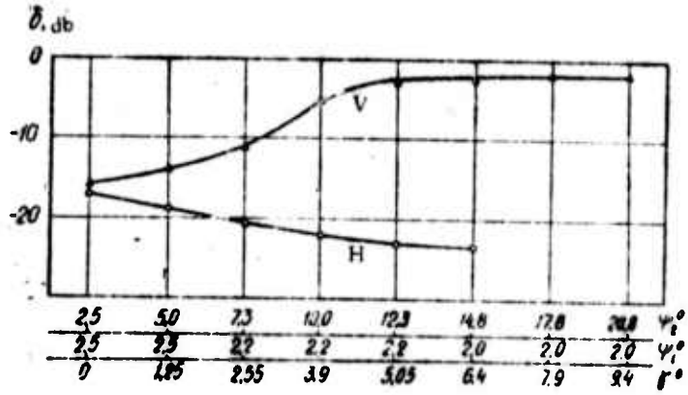

Fig. 4. The dependence on glancing angles of the degree of depolarization of scattered signals at vertical (V) and horizontal (H) polarization of emitted signals.

of emitted signals the scattered signals show a weak depolarization which decreases with an increase in ψ_2. However, the depolarization of scattered signals at vertical polarization of emitted signals increases significantly with increase in ψ_2.

The amplitude spectra of mirror reflections and scattered signals are given in Fig. 5.

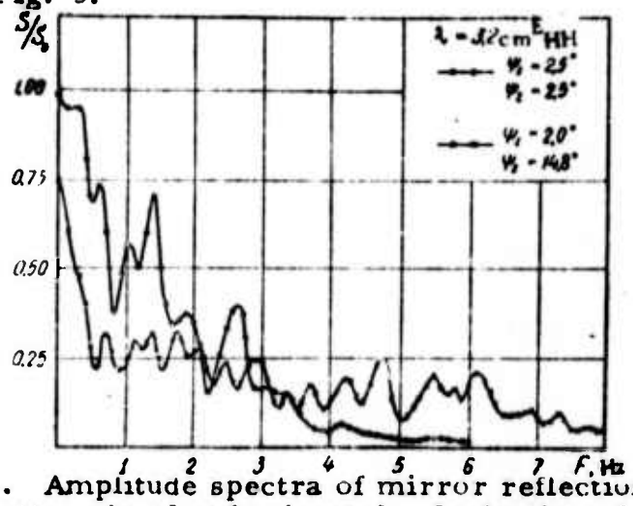

Fig. 5. Amplitude spectra of mirror reflection and scatter signal at horizontal polarization of emitted and detected signals. (Path 1)

o- mirror reflection, x- scattered signal.

The ratio of spectral widths for both mirror reflections and scattered signals with matched polarization is

$$\frac{\Delta F_{\lambda = 3.2\ cm}}{\Delta F_{\lambda = 10\ cm}} \approx 3. \qquad (1)$$

The spectra of depolarized signals are similar to those of signals with matched polarizations. The correlation coefficient for E_{VV} and E_{VH} as well as for E_{HH} and E_{HV}, is $\rho < 0.1$.

The effect of the secondary structure of sea waves was suggested as an explanation for the higher level of mirror reflections at $\lambda = 10$ cm, the depolarization of scattered signals, and broadening of scattered signal spectra.

Garnaker'yan, A. A., K. L. Afanas'yev, V. J. Lobach, and V. V. Timonov. Measuring parameters of sea waves by an airborne r-f method. Metr. i gidrol., no. 12, 1973, 102-103.

A method is described for determining ocean wave height from an aircraft, based on measurement of the ratio between coherent and incoherent components of reflected radio signals. The results of the height measurements are compared to those obtained simultaneously by the GM-16 wavegraph. The possibility is also demonstrated for the determination of wavelength and propagation direction of sea waves from the spectral width of reflected r-f signals.

The meter-band radar used in the experiment is shown in Fig. 1.

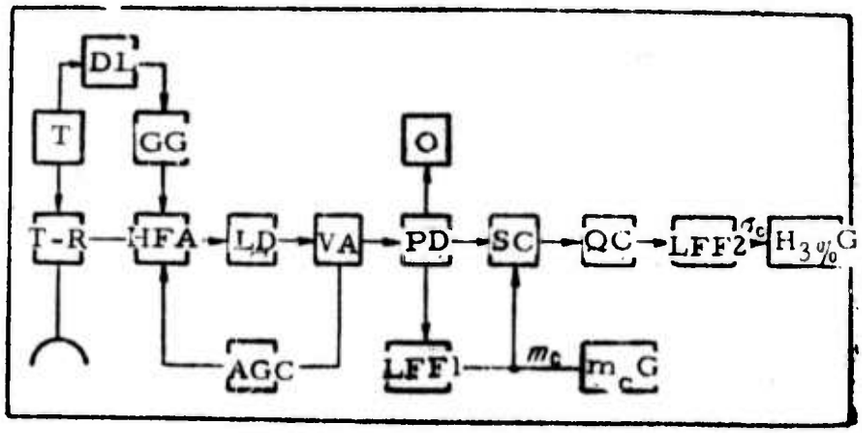

Fig. 1. Radar block diagram for measuring wave height

T-R - T-R switch; T - transmitter; DL - delay line; GG - gate generator; HFA - high-frequency amplifier; AGC - automatic gain control; LD - linear detector; VA - video amplifier; PD - peak detector; SC - subtraction circuit; QC - squaring circuit; LFF 1, 2 - low-frequency filters; m_cG - m_c meter; $H_{3\%}G$ - $H_{3\%}$ meter; O - loop oscillograph.

The radar specifications are as follows: transmitted wavelength λ = 10 m; pulse power P = 50 w; pulse duration τ = 1 μ sec; repetition rate F = 1 kHz; detector threshold u_{min} = 300μv; measured height range $H_{3\%}$ = 0-3 m.

Experiments were carried out during 1970-71 with flight altitudes of 300-3000 m, flight speeds 300-500 km/h, and various flight directions relative to the sea wave propagation line. The distance to shore was 15-20 km, water depth = 150-200 m. The experiments included direct measurements of the wave height by $H_{3\%}$-meter ($H_{3\%}G$ in Fig. 1), recording envelope of reflected signal at the output of peak detector (PD in Fig. 1) and average

value of signal at the output of low-frequency filter (LFFI in Fig. 1). An example of a recording is shown, but with no coordinate values. Some results are shown in Table 1.

Table 1

Date	Wave height by radar, cm	Wave height by wavegraph, cm
6/16/71	94	88
6/21/71	182	198
6/29/71	26	29
7/2/71	48	53
7/14/71	62	67
7/15/71	37	40
7/21/71	79	73
8/27/71	131	142

The accuracy of height measurements by the method considered depends slightly on the flight altitude, but is independent of flight speed and direction.

The calculated spectral width of reflected signals is given in Table 2.

The relation between deduced Δf and the wavelength of sea waves measured by the GM-16 wavegraph is shown in Fig. 2. The indicated dependence was suggested to be used for determining the wavelength of sea waves. For that purpose, an attachment to the peak detector measuring the average number of overshoots of the reflected signal envelope can be used (Fig. 3).

Table 2

Date	Flight direction relative to wave propagation	Spectral width Δf, Hz	$\Delta f_{\perp} / \Delta f_{\parallel}$
10/6/1970	$\perp$	4.4	2.2
	$\parallel$	2	
10/8/1970		6.8	1.7
		4	
6/16/1971		6.3	1.95
		3.2	
7/15/1971		8.8	2.4
		3.6	
8/26/1971		5.3	1.7
		3.15	
8/27/1971		6	1.8
		3.3	

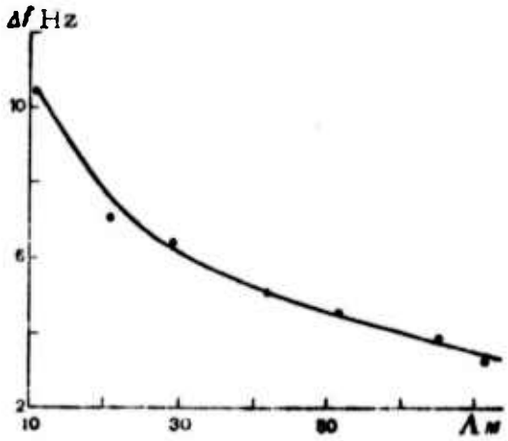

Fig. 2. Δ vs. sea wavelength.

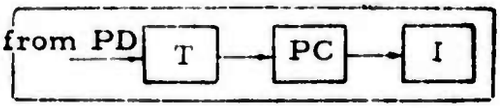

Fig. 3. Attachment to the system of Fig. 1.

PD- peak detector; T- threshold unit; PC- overshoot counter; I- indicator.

Batrakov, Yu. G. On blanking of a PPI display by r-f waves reflected from an underlying (water) surface. IN: Tr. Mosk. inta inzh. zemleustroystva. No. 63, 1973, 100-105 (RZhF, 9/73, no. 9Zh206). (Translation).

The reason is explained for occasional blanking of a 10 cm wavelength radar display during operation above a water surface. The cause of blanking is the attenuation of return signal owing to incident wave interference with the surface-reflected wave. The frequency range of blanking is evaluated at a given sensitivity of the receiver. Numerical evaluation shows that under operational conditions, this range may attain hundreds of MHz.

Timofeyev, N. A., and Ye. N. Shutova. Angular structure of the outgoing shortwave radiation field over oceans. IN: Sb. Morsk. gidrofiz. issled, no. 2(61), 1973, 132-141. (RZhGeofiz, 12/73, no. 12B234). (Translation)

The angular structure of the ocean-atmosphere brightness field is studied from data of actinometric measurements and cloud observations made during October 1969 from the "Meteor-1" and "Meteor-2" meteorological satellites. A method is introduced for converting the measured intensity of 0.3-3.0 μ radiation reflected into space to the equivalent radiation flux into a half-sphere with arbitrary atmospheric upper bound.

Babkov, A. I. An experiment in deciphering internal waves from vertical aerial photographs. IN: Aerofotos'yemka-metod izucheniya prirodnoy sredy. Izd. Nauka, Leningrad, 1973, 60-64.

A procedure is considered for identification of internal waves originating in the adjoining zone between two sea water bodies from vertical aerial photographs. The vertical aerial photograph used as an illustration (Fig. 1) was taken 4 km offshore in the Tartar Strait on September 22, 1965, at a water depth of 20 m and moderate wind wave conditions (2 ball).

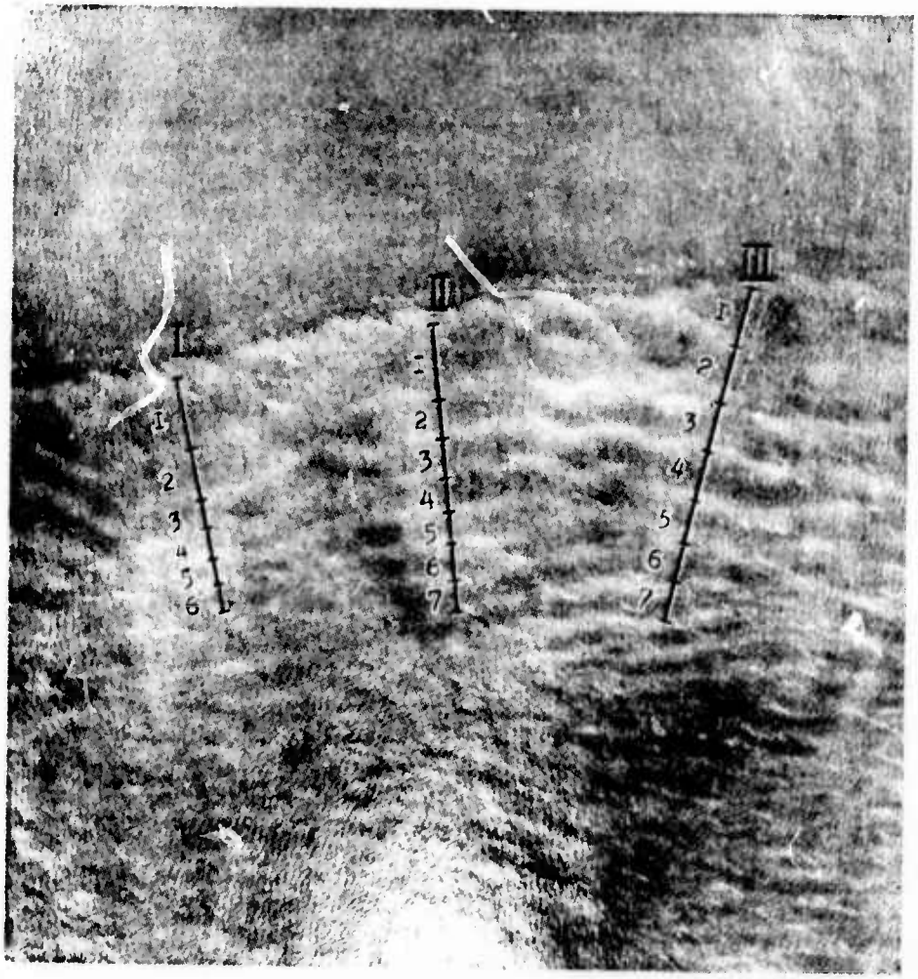

Fig. 1. Vertical aerial photograph of the boundary between different water masses, with the image of a system of internal waves.

Scale 1:5000

The following procedure was suggested:

1. Discrimination of mapped waves taking hydrometeorological conditions into account. For example, in Fig. 1 two types of waves can be discriminated: a) surface wind waves with wavelength of 4 m and propagation azimuth of 270°; b) within the region of more turbid water (lighter region in Fig. 1), waves with wavelength of 25-65 m and crests almost parallel to the boundary. The latter cannot be identified as surface wind waves.

2. Establishing that the latter waves are not caused by underwater accumulative structures. In Fig. 1 this wavelike structure is visible on only one side of the boundary. This fact, together with the shallow water depth (20 m) excludes underwater accumulative structures as a possible cause of the wavelike structure in question.

3. Analysis of the change in wavelength of the observed waves. The wavelength seen in Fig. 1 increases in the direction of the boundary, which is in agreement with Shand's data on internal waves (Shand, Trans. Amer. Geophys. Un., 34, 6, 1953).

4. Establishing differences in physical-chemical characteristics between two adjoining water masses. In the case considered, differences are indicated by the color boundary, a foam band, and by accumulation of algae and active films.

The wavelengths of the thus identified internal waves (see Table 1) were measured by the same method used for determination of surface wind waves (Sharikov, Cherkasov, 1959).

The propagation azimuth of internal waves is determined either from the aircraft course or from solar azimuth. The propagation azimuths of the internal waves shown in Fig. 1 were determined to be 302°,

Table 1

Wavelength of internal waves (in meters) along three profiles

No. of waves in Fig. 1.	Profiles		
	I	II	III
1	58.1	62.0	56.8
2	43.6	34.5	50.8
3	25.0	31.7	43.1
4	26.2	28.4	42.8
5	21.6	29.9	25.8
6	22.2	33.3	34.3
7		25.1	34.7

309° and 327° for profiles I, II and III, respectively. The corresponding wavefront azimuths are 32°, 39° and 57°.

The phase velocity of the internal waves was determined by assuming a quasistationary boundary from two overlapping photographs. The average phase velocity was thus determined to be 52 cm/sec, which agrees well with the theoretical data of Shuleykin (Fizika morya. Moskva, Izd-vo AN SSSR, 1953).

It was concluded that internal waves in a zone between two different water masses can be identified both from airborne visual observations and by using oblique and vertical aerial photographs, taking into account the hydrological characteristics of the region and photographic conditions.

Zagorodnikov, A. A. Obtaining the radar backscatter characteristic of an underlying surface from one-dimensional DME return image.
RiE, no. 2, 1974, 289-293.

The possibility is shown of reconstructing the two-dimensional radar backscatter characteristic P (x, y) of an underlying surface from one-dimensional radar return images obtained at different angles by means of a surveillance radar. This is possible with a high range-low azimuth-resolution radar, because the spatial spectrum S_p (u) of the one-dimensional image is a constant multiple of the spectral cross-section of P (x, y) for the surveyed area F (see Fig. 1). In practice, any number of one-dimensional images, and

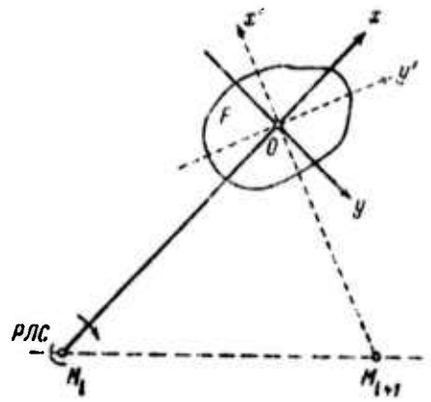

Fig. 1. Schematical one-dimensional image.

hence spectral cross-sections of P (x, y), at different angles in the $-\pi/2 \leq \theta \leq \pi/2$ range can be obtained by shifting the radar along M_i--M_{i+1} line in Fig. 1. Thus the Fourier transform $\mathfrak{F}[P(x, y)]$ can be plotted. The function P (x, y) of the area F is then calculated by the two-dimensional inverse transform

$$\mathfrak{F}^{-1}[S_p(u, v)] = \mathfrak{F}^{-1}\{\mathfrak{F}[P(x, y)]\} = P(x, y). \qquad (1)$$

In the case of a statistically rough surface, the cited method is simplified by substituting various averaged statistical characteristics, e.g. a two-dimensional energy spectrum, S_z (u, v) for the complex spectrum. A correlation analogous to that for the complex spectrum is derived between a cross-section of S_z (u, v) and the energy spectrum of the one-dimensional image S_z (u). The necessary number of S_z (u, v) cross-sections is thus determined, e.g., for a rough sea surface, by the sea's anisotropy which is evaluated from the one-dimensional angular sea spectrum $S_{z\theta}(\theta)$ in the polar coordinate system (θ, K), where $K^2 = u^2 + v^2$. Measurements of the sea states and the average size of ice fields are cited as some examples of applying the described method to statistically rough surfaces. In the first example, the extent of the return image would be 5-10 km, if a sea wavelength < 100 m is to be measured. With a shipborne radar, cross-sections of a two-dimensional sea spectrum at different θ can be obtained by turning the antenna at $\Delta\theta = \pi/2$ m intervals, where m is a characteristic of sea surface anisotropy. In the case of an ice floe, the average size of ice fields can be evaluated from a single spatial energy spectrum of a one-dimensional return image, obtained at an arbitrary angle. The cited examples show the simplicity and efficiency of the described method in application to statistically rough surfaces.

Zagorodnikov, A. A. Components of the spatial spectrum of a DME signal backscatter from a sea surface. RiE, no. 2, 1974, 419-421.

The power spectrum of a side-looking radar signal received from an underlying sea surface is analyzed statistically, to evaluate different components of the spectrum and their role in determining sea structure. The author considers a resolution area with center at 0 (x, y), subdivided into the elemental areas ΔS containing no more than one elemental backscatterer (Fig. 1).

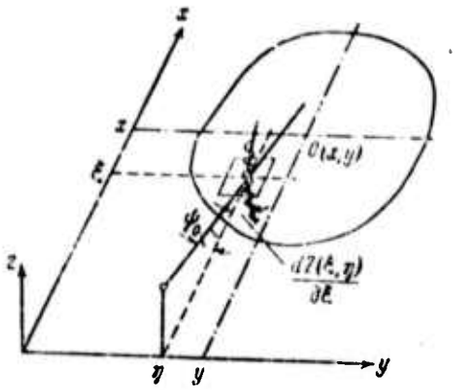

Fig. 1. Diagram of irradiated sea surface: ξ, η - coordinates of ΔS; ψ_o = glancing angle with respect to a horizontal surface: $\partial Z(\xi, \eta)/\partial \xi = \Delta\psi$ is the derivative of wave configuration in the line of sight, equal to the ΔS slope in radiation direction relative to the horizon.

The functions $E(x, y, n) \sim I^{1/2}(x, y, n)$ of the amplitude and intensity of the target envelope for an image n are expressed in terms of the ΔS size G, the slope F of irradiated wave elements, and signal phase matching. The signal I (x, y, n) which defines spatial characteristics of the sea is obtained by statistical averaging of independent images under condition of "freezing" a sea configuration, since E and I are random quantities. Hence I (x, y, n) is approximated by the sum of four components: the constant I_o, the effective I_c which is determined by the wave profile: the noise I_n, and the multiplicative component $I_m \sim I_c I_n$. For the case of a rippled sea surface $I(x, y, n) \sim q(x, y, n)$, the spatial spectrum of the function q (x, y), where q is a random quantity.

It is concluded that q (x, y, n) is equivalent to the three-dimensional white noise spectrum of a two-dimensional filter ΔS, and hence the effective and noise signal spectra always overlap in a single image. Under most favorable conditions

$$(E_c^2) \approx 0.5 E_0^2, \qquad (I_c)/I_0 = (E_c^2)/E_0^2 \approx 0.5 \tag{1},$$

$$I_m/I_0 = M_2/m_1^2 = 0.45\sigma^2/(1.25\sigma)^2 \approx 0.274 \tag{2},$$

where M_2 is the dispersion and $m_1^2 = E_0^2$, and

$$I_c I_m/I_0^2 \approx 0.5 \cdot 0.274 = 0.137. \tag{3}.$$

Thus powers of the spatial noise and the effective signal are of the same magnitude. It follows from mathematical statistics that the mean arithmetic dispersion of n independent images is lower by a factor n than dispersion of a single image. Noise can be neglected by averaging 30-50 images.

Melent'yev, V. V., and Yu. I. Rabinovich. Measuring r-f radiation from a water surface in a basin with wave generator. IN: Trudy Glavnoy geofizicheskoy observatorii, no. 295, 1973, 79-85.

This article describes multichannel measurements of r-f radiation from an agitated water surface in an artificial tank. Experiments were conducted in the wavestand shown in Fig. 1, equipped with a wave generator which could generate waves up to 220 cm high. Specifications of the stand are as follows: 1) wave basin dimensions: length - 115 m, width-r m, height - 7.5 m; water depth to 6.5 m; 2) wave parameters: height 0.5-2.2 m, length 5-40 m and period 1.8-5.8 sec.

Measurements of height, length and period of the waves were taken with two types of wave recorders, or a contact type with a spacing of 10 cm between two successive contacts, and a capacitive type.

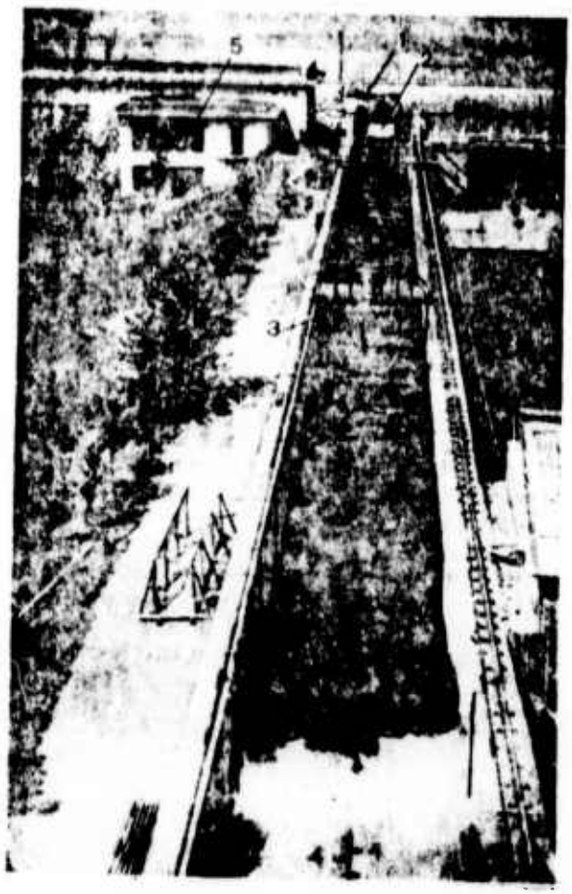

Fig. 1. Wave stand.

1 - wave generator; 2 - radiometer;
3 - wave recorder 4 - wave slope;
5 - recording instruments.

The 4-channel radiometer was located on a platform, constructed over the basin at about 30 m from the wave generator. The platform could be rotated such that r-f radiation from the water surface could be measured at different viewing angles from 0 to 70°. Measurements were conducted for a smooth water surface and for wave heights of 0.3, 0.6, 1.0, 1.5 and 2 m; the length

of waves equalled 15, 20, and 25 for a fixed wave height. R-f brightness temperatures were measured for smooth and agitated water surface at horizontal and vertical polarization, and their contrasts were calculated. Curves were drawn for r-f brightness temperatures as a function of the angle of incidence, as shown in Fig. 2. R-f brightness temperature contrast

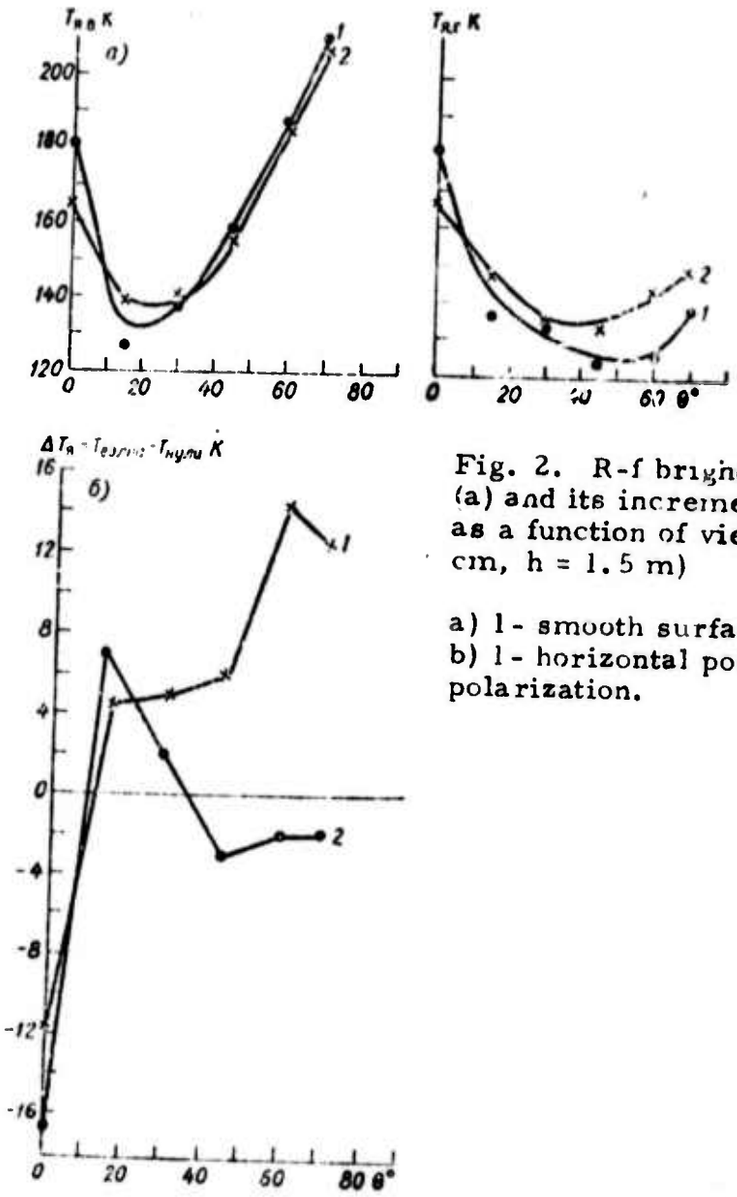

Fig. 2. R-f brightness temperature (a) and its increment due to agitation (b) as a function of viewing angle. (λ = 3.2 cm, h = 1.5 m)

a) 1 - smooth surface; 2 - wavey surface;
b) 1 - horizontal polarization; 2 - vertical polarization.

at both polarization in the basin was found to have positive values of incident angles from 10° to 35°; at large angles the brightness temperature difference between vertical and horizontal polarizations reached 14° K (Fig. 2). Experiments were conducted at r-f wavelengths of 3.2 and 0.8 cm. Comparative results showed that for the same parameters of the surface wave in the basin (height 1.5 m, wave length 30 m), the characteristic change in brightness temperature as a function of incident angle was different for different r-f wavelengths.

The authors note that r-f radiation from the water surface is affected by the noise radiation from the concrete basin walls. To avoid this effect, they suggest that the basin be covered by sheet metal and that the measurements should be conducted at maximum water level in the basin.

3. SOURCE ABBREVIATIONS

AiT	-	Avtomatika i telemekhanika
APP	-	Acta physica polonica
DAN ArmSSR	-	Akademiya nauk Armyanskoy SSR. Doklady
DAN AzSSR	-	Akademiya nauk Azerbaydzhanskoy SSR. Doklady
DAN BSSR	-	Akademiya nauk Belorusskoy SSR. Doklady
DAN SSSR	-	Akademiya nauk SSSR. Doklady
DAN TadSSR	-	Akademiya nauk Tadzhikskoy SSR. Doklady
DAN UkrSSR	-	Akademiya nauk Ukrainskoy SSR. Dopovidi
DAN UzbSSR	-	Akademiya nauk Uzbekskoy SSR. Doklady
DBAN	-	Bulgarska akademiya na naukite. Doklady
EOM	-	Elektronnaya obrabotka materialov
FAiO	-	Akademiya nauk SSSR. Izvestiya. Fizika atmosfery i okeana
FGiV	-	Fizika goreniya i vzryva
FiKhOM	-	Fizika i khimiya obrabotka materialov
F-KhMM	-	Fiziko-khimicheskaya mekhanika materialov
FMiM	-	Fizika metallov i metallovedeniye
FTP	-	Fizika i tekhnika poluprovodnikov
FTT	-	Fizika tverdogo tela
FZh	-	Fiziologicheskiy zhurnal
GiA	-	Geomagnetizm i aeronomiya
GiK	-	Geodeziya i kartografiya
IAN Arm	-	Akademiya nauk Armyanskoy SSR. Izvestiya. Fizika
IAN Az	-	Akademiya nauk Azerbaydzhanskoy SSR. Izvestiya. Seriya fiziko-tekhnicheskikh i matematicheskikh nauk

IAN B	-	Akademiya nauk Belorusskoy SSR. Izvestiya. Seriya fiziko-matematicheskikh nauk
IAN Biol	-	Akademiya nauk SSSR. Izvestiya. Seriya biologicheskaya
IAN Energ	-	Akademiya nauk SSSR. Izvestiya. Energetika i transport
IAN Est	-	Akademiya nauk Estonskoy SSR. Izvestiya. Fizika matematika
IAN Fiz	-	Akademiya nauk SSSR. Izvestiya. Seriya fizicheskaya
IAN Fizika zemli	-	Akademiya nauk SSSR. Izvestiya. Fizika zemli
IAN Kh	-	Akademiya nauk SSSR. Izvestiya. Seriya khimicheskaya
IAN Lat	-	Akademiya nauk Latviyskoy SSR. Izvestiya
IAN Met	-	Akademiya nauk SSSR. Izvestiya. Metally
IAN Mold	-	Akademiya nauk Moldavskoy SSR. Izvestiya. Seriya fiziko-tekhnicheskikh i matematicheskikh nauk
IAN SO SSSR	-	Akademiya nauk SSSR. Sibirskoye otdeleniye. Izvestiya
IAN Tadzh	-	Akademiya nauk Tadzhiksoy SSR. Izvestiya. Otdeleniye fiziko-matematicheskikh i geologo-khimicheskikh nauk
IAN TK	-	Akademiya nauk SSSR. Izvestiya. Tekhnicheskaya kibernetika
IAN Turk	-	Akademiya nauk Turkmenskoy SSR. Izvestiya. Seriya fiziko-tekhnicheskikh, khimicheskikh, i geologicheskikh nauk
IAN Uzb	-	Akademiya nauk Uzbekskoy SSR. Izvestiya. Seriya fiziko-matematicheskikh nauk
IBAN	-	Bulgarska akademiya na naukite. Fizicheski institut. Izvestiya na fizicheskaya institut s ANEB
I-FZh	-	Inzhenerno-fizicheskiy zhurnal

IiR	-	Izobretatel' i ratsionalizator
ILEI	-	Leningradskiy elektrotekhnicheskiy institut. Izvestiya
IT	-	Izmeritel'naya tekhnika
IVUZ Avia	-	Izvestiya vysshikh uchebnykh zavedeniy. Aviatsionnaya tekhnika
IVUZ Cher	-	Izvestiya vysshikh uchebnykh zavedeniy. Chernaya metallurgiya
IVUZ Energ	-	Izvestiya vysshikh uchebnykh zavedeniy. Energetika
IVUZ Fiz	-	Izvestiya vysshikh uchebnykh zavedeniy. Fizika
IVUZ Geod	-	Izvestiya vysshikh uchebnykh zavedeniy. Geodeziya i aerofotos"yemka
IVUZ Geol	-	Izvestiya vysshikh uchebnykh zavedeniy. Geologiya i razvedka
IVUZ Gorn	-	Izvestiya vysshikh uchebnykh zavedeniy. Gornyy zhurnal
IVUZ Mash	-	Izvestiya vysshikh uchebnykh zavedeniy. Mashinostroyeniye
IVUZ Priboro	-	Izvestiya vysshikh uchebnykh zavedeniy. Priborostroyeniye
IVUZ Radioelektr	-	Izvestiya vysshikh uchebnykh zavedeniy. Radioelektronika
IVUZ Radiofiz	-	Izvestiya vysshikh uchebnykh zavedeniy. Radiofizika
IVUZ Stroi	-	Izvestiya vysshikh uchebnykh zavedeniy. Stroitel'stvo i arkhitektura
KhVE	-	Khimiya vysokikh energiy
KiK	-	Kinetika i kataliz
KL	-	Knizhnaya letopis'
Kristall	-	Kristallografiya
KSpF	-	Kratkiye soobshcheniya po fizike

LZhS	-	Letopis' zhurnal'nykh statey
MiTOM	-	Metallovedeniye i termicheskaya obrabotka materialov
MP	-	Mekhanika polimerov
MTT	-	Akademiya nauk SSSR. Izvestiya. Mekhanika tverdogo tela
MZhiG	-	Akademiya nauk SSSR. Izvestiya. Mekhanika zhidkosti i gaza
NK	-	Novyye knigi
NM	-	Akademiya nauk SSSR. Izvestiya. Neorganicheskiye materialy
NTO SSSR	-	Nauchno-tekhnicheskiye obshchestva SSSR
OiS	-	Optika i spektroskopiya
OMP	-	Optiko-mekhanicheskaya promyshlennost'
Otkr izobr	-	Otkrytiya, izobreteniya, promyshlennyye obraztsy, tovarnyye znaki
PF	-	Postepy fizyki
Phys abs	-	Physics abstracts
PM	-	Prikladnaya mekhanika
PMM	-	Prikladnaya matematika i mekhanika
PSS	-	Physica status solidi
PSU	-	Pribory i sistemy upravleniya
PTE	-	Pribory i tekhnika eksperimenta
Radiotekh	-	Radiotekhnika
RiE	-	Radiotekhnika i elektronika
RZhAvtom	-	Referativnyy zhurnal. Avtomatika, telemekhanika i vychislitel'naya tekhnika
RZhElektr	-	Referativnyy zhurnal. Elektronika i yeye primeneniye

RZhF	-	Referativnyy zhurnal. Fizika
RZhFoto	-	Referativnyy zhurnal. Fotokinotekhnika
RZhGeod	-	Referativnyy zhurnal. Geodeziya i aeros"-yemka
RZhGeofiz	-	Referativnyy zhurnal. Geofizika
RZhInf	-	Referativnyy zhurnal. Informatics
RZhKh	-	Referativnyy zhurnal. Khimiya
RZhMekh	-	Referativnyy zhurnal. Mekhanika
RZhMetrolog	-	Referativnyy zhurnal. Metrologiya i izmeritel'naya tekhnika
RZhRadiot	-	Referativnyy zhurnal. Radiotekhnika
SovSciRev	-	Soviet science review
TiEKh	-	Teoreticheskaya i eksperimental'naya khimiya
TKiT	-	Tekhnika kino i televideniya
TMF	-	Teoreticheskaya i matematicheskaya fizika
TVT	-	Teplofizika vysokikh temperatur
UFN	-	Uspekhi fizicheskikh nauk
UFZh	-	Ukrainskiy fizicheskiy zhurnal
UMS	-	Ustalost' metallov i splavov
UNF	-	Uspekhi nauchnoy fotografii
VAN	-	Akademiya nauk SSSR. Vestnik
VAN BSSR	-	Akademiya nauk Belorusskoy SSR. Vestnik
VAN KazSSR	-	Akademiya nauk Kazakhskoy SSR. Vestnik
VBU	-	Belorusskiy universitet. Vestnik
VNDKh SSSR	-	VNDKh SSSR. Informatsionnyy byulleten'
VLU	-	Leningradskiy universitet. Vestnik. Fizika, khimiya
VMU	-	Moskovskiy universitet. Vestnik. Seriya fizika, astronomiya

ZhETF	-	Zhurnal eksperimental'noy i teoreticheskoy fiziki
ZhETF P	-	Pis'ma v Zhurnal eksperimental'noy i teoreticheskoy fiziki
ZhFKh	-	Zhurnal fizicheskoy khimii
ZhNiPFiK	-	Zhurnal nauchnoy i prikladnoy fotografii i kinematografii
ZhNKh	-	Zhurnal neorganicheskoy khimii
ZhPK	-	Zhurnal prikladnoy khimii
ZhPMTF	-	Zhurnal prikladnoy mekhaniki i tekhnicheskoy fiziki
ZhPS	-	Zhurnal prikladnoy spektroskopii
ZhTF	-	Zhurnal tekhnicheskoy fiziki
ZhVMMF	-	Zhurnal vychislitel'noy matematiki i matematicheskoy fiziki
ZL	-	Zavodskaya laboratoriya

4. AUTHOR INDEX